Parton Model for the Electroproduction of Single Hadrons with Highly Virtual Photons*

Probir Roy†
Laboratory of Nuclear Studies, Cornell University, Ithaca, New York 14850
(Received 24 March 1971; revised manuscript received 18 October 1971)

In this paper we study the contrasting dynamical roles played by the "wee" and the "nonwee" partons in the process $ep \to e'AB$ (A, B being hadrons) when the negative squared mass Q^2 of the virtual photon becomes large. Two relevant asymptotic limits are pointed out and are shown to be controlled by the two different parton mechanisms which are possible. In each case, one of the two final hadrons is forced to emerge predominantly in the direction of the virtual photon in the laboratory. This imposes testable kinematic restrictions for either limit. Moreover, the behavior of the structure function W_2 in these two limits is related to the square of the asymptotic electromagnetic form factor times unknown functions of the scaling variables.

I. INTRODUCTION

The parton idea of Feynman,[1] based on the application of the impulse approximation to instantaneously free pointlike constituents of a hadron in the infinite-momentum frame, is now widely known for its considerable predictive power in inclusive deep-inelastic lepton-hadron processes.[2-4] It is less commonly realized, however, that the model can lead to very interesting results for certain exclusive reactions also. In the parton description of such reactions the very soft or "wee"[5] partons play a crucial role. "Wee" partons carry a rather small fraction of the relevant hadron's momentum in the infinite-momentum frame and are of two types: (1) those carrying a fraction $m/\sqrt{s}$ of the hadron's longitudinal momentum ($\sqrt{s}$ being the c.m. energy) and (2) those carrying a fraction $\mu/\sqrt{Q^2}$ of the same ($\sqrt{Q^2}$ being the leptonic momentum transfer). Here m, μ are masses typical of the transverse-momentum cutoff seen in hadronic reactions, i.e., 400 MeV $\leq m, \mu \leq 1$ GeV. The first type of wee partons controls high-energy hadronic cross sections. The second type of wee partons is important in exclusive electromagnetic processes mediated by highly virtual photons. Drell and Yan[6] first encountered this latter kind of wee partons when they considered elastic ep scattering at large Q^2 in the parton picture. They made the important observation that, for the leading contribution to elastic ep scattering in the limit when $Q^2 \to \infty$, all of the partons in the proton except for the electromagnetically scattered one have to be wee. This enabled them to obtain a connection between the asymptotic elastic form factor $F_1(Q^2)$ and the near-threshold deep-inelastic structure function $F_2(\omega)$ of the proton; namely, if

$$\lim_{Q^2\to\infty} F_1(Q^2) = (1/Q^2)^{(p+1)/2},$$

then

$$\lim_{\omega\to 1} F_2(\omega) = \omega^{-1}(1-\omega^{-1})^p.$$

In the present paper[7] we use the approach of Ref. 6 to study single-particle electroproduction[8] at large Q^2 in the field-theoretic parton model of Drell, Levy, and Yan.[4] The process includes all reactions of the type $ep \to e'AB$ where A and B are hadrons (if these are resonances our statements will be valid only in the zero-width approximation). Certain aspects of the parton analysis of this process involve slightly stronger theoretical assumptions than those needed to consider elastic ep scattering at large Q^2. On the other hand, the kind of predictions that one can make here should be more easily testable than the Drell-Yan connection for which the experimentally difficult task of determining the *precise* form of $F_2(\omega)$ near $\omega = 1$ has to be accomplished.[6] In particular, at the time of writing, a whole range of experiments are in progress at the Cornell electron synchrotron on processes such as $ep \to p\pi^0$, $p\rho^0$, $n\pi^+$, $n\rho^+$, etc. which can hopefully test at least some of the theoretical results obtained here.

The paper is arranged in the following way. In Sec. II we discuss the kinematics of our process and set up the infinite-momentum frame for performing the parton analysis. Two different asymptotic limits that can be studied in the large-Q^2 region are discussed. In Sec. III a qualitative study of the parton dynamics in elastic ep scattering at large Q^2 is followed by the derivation of kinematic restrictions on the free variable in each of the above two asymptotic limits for single-particle electroproduction. Two different parton mechanisms are obtained and are shown to be controlling the two limits. In each case, one of the two final hadrons is predicted to emerge predominantly in the direction of the virtual photon in the laboratory. Section IV contains a review of the argu-

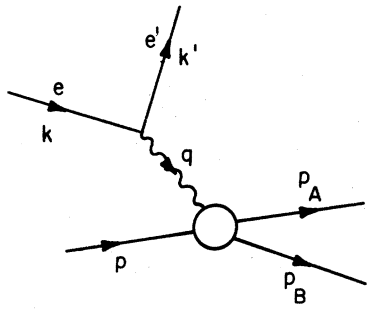

FIG. 1. Covariant description of the reaction $ep \to e'AB$.

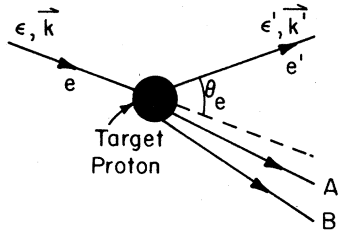

FIG. 2. Laboratory description of the reaction $ep \to e'AB$.

ment leading to the Drell-Yan[6] connection using an approach due to Yennie[9] and a discussion of the perturbation-theoretic basis of this argument. In Sec. V we set up our basic parton equation for the single-particle electroproduction amplitude with which to investigate the two asymptotic limits mentioned above. The specific form of the equation for either limit is given in terms of integrals over parton variables of suitably defined vertex functions. In Sec. VI the role of the wee partons in controlling the leading Q^2 dependence in the two limits is studied. With some reasonable theoretical assumptions the large-Q^2 behavior of the electroproduction amplitude in each of these limits is related to certain asymptotic electromagnetic form factors and the perturbation-theoretic basis of these relations is discussed. In Sec. VII the above relations are translated into predicted asymptotic forms for the structure function $\mathcal{W}_2$ in the two limits. Section VIII contains some concluding comments and summarizes our results.

II. KINEMATICS AND ASYMPTOTIC LIMITS

For the process $ep \to e'AB$, let $q = k - k'$ stand for the four-momentum carried by the virtual photon and p, p_A, and p_B for that of the proton, of A, and of B, respectively (Fig. 1). Define $Q^2 \equiv -q^2 > 0$, $\nu \equiv p\cdot q/M_P$, $\kappa_{A,B} \equiv p\cdot p_{A,B}/M_P$. Then four-momentum conservation $p+q = p_A + p_B$ and the mass-shell constraints $p^2 = M_p^2$, $p_{A,B}^2 = M_{A,B}^2$, $(p_A+p_B)^2 > (M_A+M_B)^2$ imply the following relations:

$$2M_p\nu - Q^2 > (M_A+M_B)^2 - M_p^2, \tag{2.1}$$

$$M_p^2 - Q^2 + M_{A,B}^2 - M_{B,A}^2 = 2q\cdot p_{A,B} - 2M_p(\nu - \kappa_{A,B}). \tag{2.2}$$

In the laboratory frame (Fig. 2) ϵ and $\vec{k}$, respectively, define the energy and the momentum of the incident electron and similar primed symbols define the corresponding quantities for the scattered electron, θ_e being the electron scattering angle.

In the metric (1, −1, −1, −1) and with the normalization $\langle p'|p\rangle = \delta^{(3)}(\vec{p}' - \vec{p})$, our scattering amplitude is

$$S_{fi} = \left(\frac{1}{2\pi}\right)^3 \left(\frac{m_e^2}{\epsilon\epsilon'}\right)^{1/2} i(2\pi)^4\delta^{(4)}(p+q-p_A-p_B) \times e^2\bar{u}_e(k')\gamma^\mu u_e(k)\frac{1}{q^2+i\epsilon}\langle p_A, p_B|J_\mu|p\rangle. \tag{2.3}$$

In Eq. (2.3) J_μ stands for the hadronic electromagnetic current. If, when a final hadron J (this can be either A or B) is detected, the azimuthal angle ϕ_J associated with d^3p_J in the laboratory frame is integrated away, then for the triple-differential cross section in the laboratory frame we have (cf. Ref. 4, first paper)

$$\frac{d^3\sigma}{d\epsilon' d\cos\theta_e dE_J} = \frac{4\pi\alpha^2}{Q^4}\frac{\epsilon'}{\epsilon}(k^\mu k'^\nu + k'^\mu k^\nu + \tfrac{1}{2}q^2 g^{\mu\nu}) \times \int d^3p_B \int d^3p_A \delta\left(\kappa_J - \frac{p\cdot p_J}{M_p}\right)(2\pi)^6\delta^{(4)}(p+q-p_A-p_B)\overline{\sum_{\text{spins}}}\langle p|J_\mu(0)|p_A,p_B\rangle\langle p_B,p_A|J_\nu(0)|p\rangle. \tag{2.4}$$

In Eq. (2.4) the symbol $\overline{\sum}_{\text{spins}}$ implies that the initial spins are being averaged and the final spins summed. Noting that Q^2, ν, and κ_J can be taken to be the three independent variables, we introduce two structure functions $\mathcal{W}_1(Q^2,\nu,\kappa_J)$ and $\mathcal{W}_2(Q^2,\nu,\kappa_J)$ via the relation

$$\frac{p_0}{M_p}\int d^3p_B\int d^3p_A\delta\left(\kappa_J - \frac{p\cdot p_J}{M_p}\right)(2\pi)^6\delta^{(4)}(p+q-p_A-p_B)\overline{\sum_{\text{spins}}}\langle p|J_\mu(0)|p_A,p_B\rangle\langle p_B,p_A|J_\nu(0)|p\rangle = \mathcal{W}_{\mu\nu} = \mathcal{W}_1(Q^2,\nu,\kappa_J)\left(-g_{\mu\nu}+\frac{q_\mu q_\nu}{q^2}\right) + \frac{1}{M_p^2}\mathcal{W}_2(Q^2,\nu,\kappa_J)\left(p_\mu - \frac{p\cdot q}{q^2}q_\mu\right)\left(p_\nu - \frac{p\cdot q}{q^2}q_\nu\right). \tag{2.5}$$

Now Eq. (2.4) can be cast in the following convenient form:

$$\frac{d^3\sigma}{dQ^2 d\nu d\kappa_J} = \frac{4\pi\alpha^2}{Q^4}\frac{\epsilon'}{\epsilon}\left[\mathfrak{W}_2 \cos^2(\tfrac{1}{2}\theta_e) + 2\mathfrak{W}_1 \sin^2(\tfrac{1}{2}\theta_e)\right]. \tag{2.6}$$

There are two asymptotic limits for single-particle electroproduction at large Q^2 that are of interest in the present parton analysis:

(1) Fixed-ω limit (Bjorken limit): Here $\nu \to \infty$ and $Q^2 \to \infty$ in such a way that the ratio $2M_p\nu/Q^2 \equiv \omega$ is kept fixed at some value >1. In this limit there is no *a priori* kinematic constraint on κ_J except that it has to be in the range $M_J \leq \kappa_J \leq \nu$.

(2) Fixed-τ_J limit: Here $\nu \to \infty$ and $\kappa_J \to \infty$ in such a way that the ratio $\kappa_J/\nu = \tau_J$ is kept fixed at some value <1. In this limit Q^2 can, *a priori*, have any large (for the parton analysis to be valid) positive value bounded by $2M_p\nu$.

The parton analysis has to be performed in a suitable infinite-momentum frame. Following Ref. 6, we choose the frame with $P \to \infty$ in which

$$\begin{aligned} p^\mu &= (P + M_p^2/2P, 0, 0, P), \\ q^\mu &= (M_p\nu/P, \vec{q}_\perp, 0), \\ q_\perp^2 &= Q^2 + O(1/P^2). \end{aligned} \tag{2.7}$$

Here the longitudinal direction is that of the proton's momentum and $\vec{q}_\perp$ is a transverse vector such that the large-Q^2 limit corresponds to $q_\perp \to \infty$ in this frame. As has been discussed in Ref. 3, the assumptions of the parton model are implemented in processes with highly virtual photons by taking P first to infinity with $q_\perp$ fixed, and then letting $q_\perp$ go to ∞. The four-momentum of each final hadron in this frame can be described as

$$p_J^\mu = (X_J P + (M_J^2 + k_{J\perp}^2)/2X_J P, \vec{k}_{J\perp}, X_J P), \tag{2.8}$$

where $\vec{k}_{J\perp}$ is a transverse vector and X_J a scalar. Now from the definition of κ_J, we have

$$\kappa_J \equiv \frac{p\cdot p_J}{M_p} = \frac{X_J M_p}{2} + \frac{M_J^2 + k_{J\perp}^2}{2X_J M_p}. \tag{2.9}$$

On the other hand, momentum and energy conservation imply

$$X_A + X_B = 1, \tag{2.10a}$$

$$\vec{k}_{A\perp} + \vec{k}_{B\perp} = \vec{q}_\perp, \tag{2.10b}$$

$$M_p^2 + 2M_p\nu = \frac{M_A^2 + k_{A\perp}^2}{X_A} + \frac{M_B^2 + k_{B\perp}^2}{X_B}. \tag{2.10c}$$

The relations (2.9) and (2.10) will be sufficient for our purposes to determine X_J, $\vec{k}_{J\perp}$ in terms of the observables Q^2, ν, and κ_J.

The final remark that we want to make in this section is that for leading single-particle electroproduction at large Q^2 in the parton model (at either of the two asymptotic limits mentioned above) one of the final hadrons will be shown to emerge predominantly in the direction of the virtual photon. *Henceforth we shall refer to this particle as A.* It is to be noted that some of the most interesting results of the parton model will directly involve the kinematic variables of this particle. Hence in order to test the results of the parton model experimentally, it would be *convenient* (although by no means necessary) to detect a final hadron in the direction of the electron's momentum transfer. During the rest of the paper we shall therefore write down all our formulas simply replacing the subscript J by A, the extension of our considerations to the case where B is detected being quite straightforward.

III. KINEMATIC RESTRICTIONS FROM PARTON DYNAMICS

The kinematic restrictions following from the parton model for single-particle electroproduction at large Q^2 are restrictions on the behavior of the free variables in each asymptotic limit. Thus – for leading contributions to the fixed-ω limit – the variable κ_A will be forced to behave in a constrained way that is observable; the same is true for the variable Q^2 in the fixed-τ_A limit. In order to understand these restrictions, it is instructive to begin by making a qualitative study of the parton dynamics of elastic ep scattering at large Q^2 as considered by Drell and Yan[6] (Fig. 3). The point of utmost importance in this case is that for the leading contribution all the parton constituents of the proton except the electromagnetically scattered one have to be wee. This is a necessary consequence of the basic requirement of the finiteness[10] of the transverse momenta involved in any hadronic vertex with partons even in the $q_\perp \to \infty$ limit, as can be seen in the following way. Let the ith parton in the undressed proton in Fig. 3 have the four-momentum

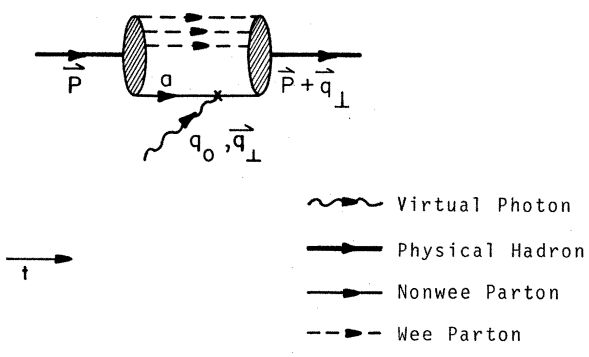

FIG. 3. Large-momentum-transfer elastic ep scattering in the Drell-Yan parton picture.

$$p_i^{\mu} = (\eta_i P + (\mu_i^2 + k_{i\perp}^2)/2\eta_i P, \vec{k}_{i\perp}, \eta_i P), \qquad (3.1)$$

where η_i is its fraction of the total longitudinal momentum $\vec{P}$ and $\vec{k}_{i\perp}$ its transverse momentum; $\sum_i \eta_i = 1$ and $\sum_i \vec{k}_{i\perp} = 0$. The transverse momenta are all kept under a cutoff.[10] Let a be the electromagnetically scattered constituent and μ be some mass of the order of the $k_\perp$ cutoff. On being scattered by the virtual photon, the parton a combines with the unscattered bunch in the redressing vertex in Fig. 3 to give back a final physical proton of momentum $\vec{P} + \vec{q}_\perp$. Just before the redressing, the momentum of the unscattered bunch is

$$\vec{p}_u = (1 - \eta_a)\vec{P} + \sum_{j \neq a} \vec{k}_{j\perp}$$

and that of the scattered constituent is $\vec{p}_s = \eta_a \vec{P} + \vec{k}_{a\perp} + \vec{q}_\perp$ where $\vec{k}_{a\perp} = -\sum_{j \neq a} \vec{k}_{j\perp}$. We rewrite these as

$$\begin{aligned} \vec{p}_u &= (1 - \eta_a)(\vec{P} + \vec{q}_\perp) - (1 - \eta_a)\vec{q}_\perp + \sum_{j \neq a} \vec{k}_{j\perp}, \\ \vec{p}_s &= \eta_a(\vec{P} + \vec{q}_\perp) + (1 - \eta_a)\vec{q}_\perp - \sum_{j \neq a} \vec{k}_{j\perp}. \end{aligned} \qquad (3.2)$$

It is clear that relative to the final-proton's momentum $\vec{p}_s + \vec{p}_u = \vec{P} + \vec{q}_\perp$, all transverse momenta can remain finite in the redressing vertex as $q_\perp \to \infty$ only if $\lim_{q_\perp \to \infty}(1 - \eta_a)q_\perp$ is finite. In other words

$$\eta_a \simeq 1 - \mu/q_\perp$$

and (3.3)

$$\eta_j = (\mu/q_\perp)x_j \quad (j \neq a),$$

where $\sum_{j \neq a}^{l} x_j = 1$. This means that only the a parton is "nonwee" and the rest are "wee." (Note that if large-Q^2 elastic electron scattering of a hadron is controlled by the wee partons, one is inclined to expect the asymptotic form factors of all hadrons to fall off with the same power of Q^{-2}. In other words, the leading power of Q^{-2} is controlled totally by the wee partons being emitted and absorbed and not by the external particles. This is the point of view that we shall adopt.)

In the reaction $ep \to eAB$ some interaction is necessary[11] between the electromagnetically scattered parton of momentum $\vec{p}_s$ and the unscattered bunch to produce two final hadrons. Let us consider, for example, the situation depicted in Fig. 4. The initial proton is undressed into partons of which one is electromagnetically scattered. The scattered parton decays at the A vertex into the physical particle A and some other partons (call this bunch α). The latter combine with the originally unscattered partons (henceforth called bunch β) at the B vertex to give the physical particle B. Of course, energy is conserved at neither of these vertices since we look at a time-ordered diagram; there is only over-all energy conservation. At the A vertex let the particle A take up a fraction χ (≤ 1) of the momentum of the decaying parton, whereas let the other fraction be carried off by the bunch α. For the momenta of the physical particle A and of the bunch α, respectively, we can then write

$$\begin{aligned} \vec{p}_A &= \chi \vec{p}_s + \vec{p}' \\ &= \chi(\eta_a \vec{P} + \vec{q}_\perp) + \chi \vec{k}_{a\perp} + \vec{p}' \end{aligned} \qquad (3.4a)$$

and

$$\vec{p}_\alpha = (1 - \chi)\vec{p}_s - \vec{p}', \qquad (3.4b)$$

where $\vec{p}'$ is defined as the vector transverse to $\vec{p}_s = \eta_a \vec{P} + \vec{k}_{a\perp} + \vec{q}_\perp$. The requirement of the finiteness (as $q_\perp \to \infty$) of the transverse momenta (relative to $\vec{p}_s$) at the A vertex simply means that p' is finite. Note that Eqs. (2.8) and (3.4a) imply

$$X_A = \chi \eta_a \qquad (3.5a)$$

and

$$\vec{k}_{A\perp} \simeq \chi \vec{q}_\perp + \text{finite}. \qquad (3.5b)$$

At the B vertex, on the other hand, the combining momenta are

$$\begin{aligned} \vec{p}_\alpha &= (1 - \chi)\vec{p}_s - \vec{p}' \\ &= (1 - \chi)(\eta_a \vec{P} + \vec{q}_\perp) + (1 - \chi)\vec{k}_{a\perp} + \vec{p}' \end{aligned} \qquad (3.6a)$$

and

$$\vec{p}_\beta = (1 - \eta_a)\vec{P} - \vec{k}_{a\perp}. \qquad (3.6b)$$

Hence the momentum of the physical particle B is finally given by $\vec{p}_B = \vec{p}_\alpha + \vec{p}_\beta$, i.e.,

$$\vec{p}_B = (1 - \eta_a \chi)\vec{P} - \chi \vec{k}_{a\perp} + (1 - \chi)\vec{q}_\perp - \vec{p}'. \qquad (3.7)$$

From Eqs. (3.6) and (3.7) it should be clear that the requirement of finite (as $q_\perp \to \infty$) transverse momenta at the B vertex with respect to $\vec{p}_B$ can be satisfied only in two ways: (1) $\chi \sim 1 - \mu/q_\perp$ as

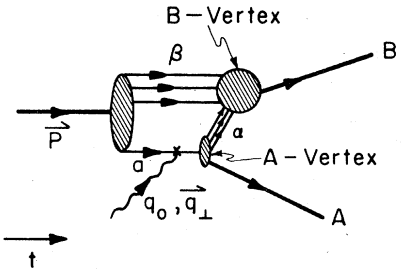

FIG. 4. Interaction between the electromagnetically scattered parton and the unscattered bunch in the reaction $ep \to e'AB$.

$q_\perp \to \infty$, i.e., the bunch α consists of wee partons only, and (2) $\eta_a \sim 1 - m/q_\perp$ as $q_\perp \to \infty$, i.e., the bunch β consists of wee partons only. The first case corresponds to wee-parton exchanges between the A vertex and the B vertex. There is clearly no reason why these wee partons should only go from the A to the B vertex. The more general situation of this type is shown in Fig. 5 where wee partons go from either of the two vertices to the other one (everything, of course, moves forward[12] with time). We will show that this picture describes the fixed-ω limit properly. The second case corresponds to nonwee-parton exchanges between the vertices A and B; but all the partons produced at the initial proton-undressing vertex except the electromagnetically scattered one are now wee. Hence in this case any interaction between the A vertex and the B vertex via nonwee-parton exchanges can be possible only if these nonwee partons move from the former to the latter. We will show that this picture correctly describes the fixed-τ_A limit.

Let us now discuss the above two cases in detail:

Case 1 (Fig. 5). Let the group of wee partons moving from the B vertex to the A vertex bring in a total momentum of $(\chi_1 - 1)(\eta_a \vec{P} + \vec{k}_{a\perp} + \vec{q}_\perp) + \vec{p}\,'_1$ to the former. Similarly, let those going from the A vertex to the B vertex take away a total momentum of $(1-\chi_2)\chi_1(\eta_a \vec{P} + \vec{k}_{a\perp} + \vec{q}_\perp) + \vec{p}\,'_2$ from the same. Here $\chi_1 \sim 1 + \mu_1/q_\perp$, $\chi_2 \sim 1 - \mu_2/q_\perp$, $\mu_{1,2} \sim k_\perp$ cutoff, $\vec{p}\,'_{1,2} \cdot (\eta_a \vec{P} + \vec{k}_{a\perp} + \vec{q}_\perp) = 0$, and $p'_{1,2}$ are finite. Now Eqs. (3.4a) and (3.7) are still valid in this more general situation provided we write $\chi = \chi_1\chi_2 \sim 1 + (\mu_1 - \mu_2)q_\perp^{-1}$ and $\vec{p}\,' = \vec{p}\,'_1 - \vec{p}\,'_2$. Also, since from Eqs. (3.4a) and (2.8)

$$\vec{k}_{A\perp} \underset{q_\perp \to \infty}{\sim} [1 + (\mu_1 - \mu_2)q_\perp^{-1}](\vec{k}_{a\perp} + \vec{q}_\perp) + \text{finite}\,,$$

we have

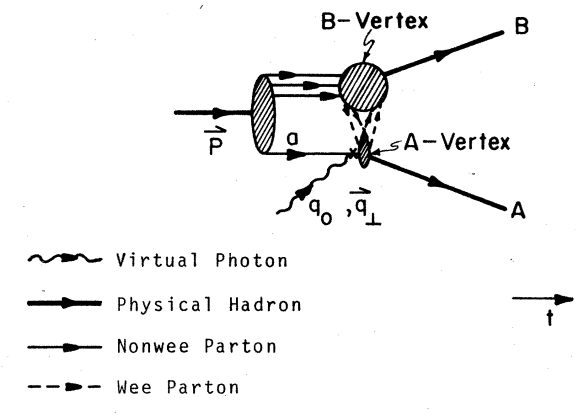

FIG. 5. Single-particle electroproduction in the fixed-ω (Bj) limit.

$$\lim_{q_\perp \to \infty} \frac{k_{A\perp} - q_\perp}{q_\perp} = O(1/q_\perp)\,. \tag{3.8}$$

Substituted in Eqs. (2.10c), this implies that in the large-Q^2 limit one has

$$\lim_{q_\perp \to \infty} X_A = \frac{Q^2}{2M_p\nu} + O(1/\sqrt{Q^2})\,. \tag{3.9}$$

On the other hand, from Eqs. (3.4a) and (2.8), once again, we have

$$X_A \underset{q_\perp \to \infty}{\sim} [1 + (\mu_1 - \mu_2)q_\perp^{-1}]\eta_a$$

so that we get

$$\eta_a = \lim_{q_\perp \to \infty} X_A = \frac{Q^2}{2M_p\nu} + O(1/\sqrt{Q^2})\,. \tag{3.10}$$

In this case, however, η_a – the fraction of the longitudinal momentum carried by the electromagnetically scattered parton in the $P \to \infty$ frame – is some finite number in the range $0 < \eta_a < 1$. Hence this case corresponds to that large-Q^2 limit, where $2M_p\nu/Q^2 = \omega$ is fixed [i.e., the Bjorken (Bj) limit] and we have

$$\lim_{\text{Bj}} X_A = \eta_a = 1/\omega + O(1/\sqrt{Q^2})\,. \tag{3.11}$$

Now Eqs. (3.8) and (3.11) imply, in conjunction with Eqs. (2.9) and (2.2), that

$$\lim_{\text{Bj}} \frac{\kappa_A}{\nu} = \lim_{\text{Bj}} \frac{2q \cdot p_A}{-Q^2} = 1 + O(1/\sqrt{Q^2})\,. \tag{3.12}$$

Thus the free variable of the Bj limit, i.e., κ_A, is forced by parton dynamics to tend to ν in the leading terms. Moreover, if θ_A is the laboratory angle between the momentum $\vec{p}_A$ of the particle A and that of the virtual photon $\vec{q}$, Eq. (3.12) implies that[13]

$$\lim_{\text{Bj}}(1 - \cos\theta_A) = O(1/\sqrt{\nu^3})\,, \tag{3.13}$$

i.e., in the fixed-ω limit A should come out mostly in the laboratory direction of the virtual photon, as claimed in Sec. II.

Case 2 (Fig. 6). This case can be considered using arguments analogous to those given above. Now $\eta_a \sim 1 - m/q_\perp$ as $q_\perp \to \infty$, where $m \sim k_\perp$ cutoff and

$$\vec{p}_A \underset{q_\perp \to \infty}{\sim} \chi(\vec{P} + \vec{q}_\perp) + \chi\vec{k}_{a\perp} + \text{finite}\,. \tag{3.14}$$

From Eqs. (2.8) and (3.14) we have

$$\lim_{q_\perp \to \infty} X_A = \chi + O(1/\sqrt{Q^2})$$

and (3.15)

$$\lim_{q_\perp \to \infty} \vec{k}_{A\perp} = \chi\vec{q}_\perp + \text{finite}\,.$$

Substituted in Eq. (2.9), Eqs. (3.15) imply

$$\lim_{q_\perp\to\infty}\frac{\kappa_A}{\nu}=\frac{\chi Q^2}{2M_p\nu}+O(1/\sqrt{\nu})\,. \tag{3.16}$$

On the other hand, Eqs. (2.10c) and (3.15) lead to the result

$$\lim_{q_\perp\to\infty}\frac{Q^2}{2M_p\nu}=1+O(1/\sqrt{Q^2}) \tag{3.17}$$

which, combined with Eq. (3.16), yields

$$\lim_{q_\perp\to\infty}\frac{\kappa_A}{\nu}=\chi+O(1/\sqrt{Q^2})\,. \tag{3.18}$$

For the present case, χ – the fraction of the momentum of the electromagnetically scattered parton carried off by the particle A at the A vertex – is a finite number in the range $0<\chi<1$. Thus now we have the limit where $\kappa_A/\nu=\tau_A$ is fixed so that $\lim_{\tau_A}\chi=\tau_A+O(1/\sqrt{Q^2})$. Equation (3.17) is the parton restriction on the free variable Q^2 in this limit. Substituting this in Eq. (2.2) we obtain $\lim_{\tau_A} q\cdot p_A/-M_p\nu=\tau_A+O(1/\sqrt{\nu})$ which implies[13] that once again, in the laboratory frame, we have

$$\lim_{\tau_A}(1-\cos\theta_A)=O(1/\sqrt{\nu^3}) \tag{3.19}$$

and that A comes out mostly in the direction of the electron's momentum transfer in this case,

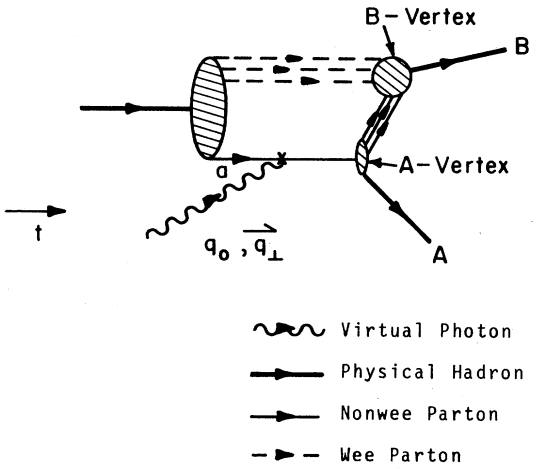

FIG. 6. Single-particle electroproduction in the fixed-τ_A limit.

too. Moreover, Eqs. (3.15) now become

$$\lim_{\tau_A} X_A=\tau_A+O(1/\sqrt{Q^2})$$

and

$$\lim_{\tau_A}\vec{k}_{A\perp}=\tau_A\vec{q}_\perp+\text{finite}\,. \tag{3.20}$$

IV. DRELL-YAN RELATION BETWEEN DEEP-INELASTIC AND ELASTIC *ep* SCATTERING

In this section we review the argument of Drell and Yan[6] that led to a connection (see Sec. I) between the proton's elastic form factor $F_1(Q^2)$ at large Q^2 and its deep-inelastic structure function $F_2(\omega)$ near the threshold $\omega\simeq 1$. This review will be useful when we use similar arguments to relate the large-Q^2 behavior of our structure function $\mathcal{W}_2$ to the asymptotic electromagnetic form factor. The authors of Ref. 6 start by undressing with the unitary U matrix the physical proton of momentum $\vec{P}$ (in the infinite-momentum frame) into bare partons:

$$|Up\rangle=\sqrt{Z_2}\,|p\rangle+\sum_{l=1}^{\infty}\int\prod_{i=1}^{l+1}d^3k_i\,|\vec{k}_1\cdots\vec{k}_{l+1}\rangle\frac{f_p^l(\vec{k}_1,\ldots,\vec{k}_{l+1})}{\sqrt{P^l}}\,\delta^{(3)}\Big(\sum_i^{l+1}\vec{k}_i-\vec{P}\Big)\,. \tag{4.1}$$

In Eq. (4.1), f_p^l, the vertex function associated with undressing the proton into $l+1$ partons, is given by

$$\frac{f_p^l(\vec{k}_1,\ldots,\vec{k}_{l+1})}{\sqrt{P^l}}\,\delta^{(3)}\Big(\sum_i^{l+1}\vec{k}_i-\vec{P}\Big)=\langle\vec{k}_1\cdots\vec{k}_{l+1}|\,Up\rangle\,. \tag{4.2}$$

Z_2 – the wave-function renormalization constant of the proton – has to be set equal to zero[14] to ensure the absence of any pointlike behavior in large-Q^2 elastic ep scattering. The normalization $\langle Up'|\,Up\rangle=\delta^{(3)}(\vec{P}'-\vec{P})$ is maintained by the condition

$$1=\sum_{l=1}^{\infty}\int\prod_{i=1}^{l+1}d^3k_i\,\frac{|f_p^l(\vec{k}_1,\ldots,\vec{k}_{l+1})|^2}{P^l}\,\delta^{(3)}\Big(\sum_i^{l+1}\vec{k}_i-\vec{P}\Big)\,. \tag{4.3}$$

To obtain a parton-model expression for $F_2(\omega)$, Drell and Yan[6] rewrite J_μ in terms of the bare current j_μ by $J_\mu(0)=U^{-1}j_\mu(0)U$, choose just the good components ($\mu=0,3$) so that only partons moving forward in the $P\to\infty$ frame are relevant,[12] and use the free-parton approximation. Then one has

$$\lim_{\text{Bj}}\Big[W_1(Q^2,\nu)\Big(-g_{\mu\nu}+\frac{q_\mu q_\nu}{q^2}\Big)+\frac{W_2(Q,\nu)}{M_p^{\,2}}\Big(p_\mu-\frac{p\cdot q}{q^2}q_\mu\Big)\Big(p_\nu-\frac{p\cdot q}{q^2}q_\nu\Big)\Big]=-\frac{4\pi^2}{M_p}p_0\int d^4x\,e^{iq\cdot x}\langle Up\,|j_\mu(x)j_\nu(0)\,|Up\rangle\,. \tag{4.4}$$

In Eq. (4.4) one can substitute the expression for $|Up\rangle$ from Eq. (4.1) and use the Born result

$$4\pi^2\int d^4x\, e^{iq\cdot x}\langle \vec{p}_1\cdots\vec{p}_{m+1}|j^\mu(x)j^\nu(0)|\vec{k}_1\cdots\vec{k}_{l+1}\rangle = \sum_a \frac{\lambda_a^{\,2}}{2k_a^0}\,\delta_{ml}(-g^{\mu\nu}Q^2+4k_a^\mu k_a^\nu+\cdots)\delta(q^2+2k_a\cdot q)$$
$$\times\,\delta^{(3)}(\vec{p}_1-\vec{k}_1)\cdots(\text{excluding } a\text{th factor})\cdots\delta^{(3)}(\vec{p}_{l+1}-\vec{k}_{l+1}),$$

where λ_a is the charge of the scattered constituent a. If we call the fraction of the longitudinal momentum carried by the ith parton η_i, then in this frame $k_a^\mu \simeq \eta_a P^\mu$ + nonleading terms. Thus one obtains [see Eq. (78) in the second paper of Ref. 3]

$$\lim_{\text{Bj}} \nu W_2(Q^2,\nu) = F_2(\omega) \equiv \sum_{l=1}^{\infty}\sum_a F_{2l}^a(\omega),$$

where

$$F_{2l}^a(\omega) = \frac{\lambda_a^{\,2}}{\omega}\int\prod_{i=1}^{l} d^2k_{i\perp}d\eta_i\,\theta\Big(1-\sum_{i=1}^{l}\eta_i\Big)\,\delta(\eta_a-1/\omega)\,|f_p^l(\cdots\eta_i\cdots;\cdots\vec{k}_{i\perp}\cdots)|^2. \tag{4.5}$$

Similarly, starting from $(2\pi)^3\langle Up'|j^{0,3}|Up\rangle_{\text{spin av.}} = F_1(Q^2)$ and using

$$(2\pi)^3\langle\vec{k}_1'\cdots\vec{k}_{m+1}'|j^{0,3}|\vec{k}_1\cdots\vec{k}_{l+1}\rangle = \delta_{lm}\sum_a\lambda_a\delta^{(3)}(\vec{k}_1'-\vec{k}_1)\cdots(\text{except } a\text{th factor})\cdots\delta^{(3)}(\vec{k}_{m+1}'-\vec{k}_{l+1}) \tag{4.6}$$

we get[6]

$$\lim_{Q^2\to\infty} F_1(Q^2) = \sum_{i=1}^{\infty}\sum_a F_{1l}^a(Q^2),$$

where

$$F_{1l}^a(Q^2) = \lambda_a\int\prod_{i=1}^{l} d^2k_{i\perp}d\eta_i\,\theta\Big(1-\sum_i^l\eta_i\Big)f_{p'}^{l\,*}(\eta_i;\vec{k}_{1\perp}-\eta_1\vec{q}_\perp,\ldots,\vec{k}_{a\perp}+(1-\eta_a)\vec{q}_\perp,\ldots,\vec{k}_{l\perp}-\eta_l\vec{q}_\perp)f_p^l(\eta_i;\vec{k}_{i\perp}). \tag{4.7}$$

Here f_p^l and $f_{p'}^l$ are vertex functions associated with the initial undressing and the final redressing vertices of the proton, respectively.

The Drell-Yan connection, which can strictly be established only between $F_{2l}^a(\omega)$ and $F_{1l}^a(Q^2)$ and then conjectured to hold between $F_2(\omega)$ and $F_1(Q^2)$, becomes particularly transparent in an argument due to Yennie.[9] In Eq. (4.7) substitute η_j for $j\neq a$ by $\mu q_\perp^{-1}x_j$ in accordance with the second of Eqs. (3.3). In the η_a integration, we write

$$\eta_a = 1-\frac{\mu' z_a}{q_\perp},$$

where $\mu'\sim\mu$ (cf. Sec. III). Thus, in the $q_\perp\to\infty$ limit, because of the first of Eqs. (3.3), we can write

$$\int_0^1 d\eta_a \simeq \frac{\mu'}{q_\perp}\int_0^{\text{finite}} dz_a$$

and replace η_a by 1 everywhere in the integrand. Now Eq. (4.7) becomes

$$\lim_{q_\perp\to\infty} F_{1l}^a(q^2) \simeq \lambda_a\Big(\frac{\mu}{q_\perp}\Big)^l\int_0^{\text{fin}} dz_a\int d^2k_{a\perp}\prod_{j\neq a}^{l-1}\int_0^1 dx_j\int d^2k_{j\perp}\,\theta\Big(z_a-\sum_{j\neq a}^{l-1}x_j\Big)f_{p'}^{l\,*}f_p^l. \tag{4.8}$$

In Eq. (4.8)

$$f_p^l \equiv f_p^l(1,\mu x_j q_\perp^{-1};\ldots),$$
$$f_{p'}^l \equiv f_{p'}^l(1,\mu x_j q_\perp^{-1};\ldots).$$

These functions have the same longitudinal variables, but their finite transverse variables are different by finite amounts $\sim\mu\hat{q}_\perp$. It is reasonable to assume that the finite transverse variables do not play an important role in controlling the $q_\perp$ dependence of $F_{1l}^a(q_\perp)$. Now one can rewrite $F_{2l}^a(\omega)$ of Eq. (4.5) in a similar manner by substituting $1-\eta_a = x_a(1-\omega^{-1})$ and $\eta_j = x_j(1-\omega^{-1})$ for $j\neq a$. Then one has

$$F_{2l}^a(\omega) = \lambda_a{}^2\omega^{-1}(1-\omega^{-1})^{l-1}\prod_{i=1}^{l}\int d^2k_{i\perp}\int_0^\infty dx_i$$
$$\times\,\theta\Big(x_a-\sum_{j\neq a}x_j\Big)\,\theta\Big(\frac{1}{1-\omega^{-1}}-x_a\Big)|f_p^l|^2. \tag{4.9}$$

Once again $\int_0^\infty dx_a \to \int_0^{\text{fin}} dx_a$ and, as $\omega\to 1$, $\theta(1/(1-\omega^{-1})-x_a)$ can be taken =1. Now the argument of f_p^l in Eq. (4.9) is the same as that in Eq. (4.8) except that $\mu q_\perp^{-1}$ is replaced by $1-\omega^{-1}$ everywhere. Thus the leading powers of these variables emanating from the integrals of Eqs. (4.8) and (4.9) should be the same. Hence the leading power of $\mu q_\perp^{-1}$ in $F_{1l}^a(q_\perp)$ is expected

to be greater than that of $1-\omega^{-1}$ in $F_{2I}^{a}(\omega)$ by one in the respective limits $q_\perp \to \infty$ and $\omega \to 1$ while there is an additional factor of ω^{-1} in $F_{2I}^{a}(\omega)$. This is what leads to the Drell-Yan[6] connection.

Drell and Yan have verified that their conjecture is valid (by a diagram-by-diagram analysis) to any finite order in old-fashioned perturbation theory so long as the virtual transverse momenta are kept finite. They take a model[3] of 0^- mesons and $\frac{1}{2}^+$ baryons with a γ_5 coupling and a transverse-momentum cutoff. In this model, to every order, the diagrams contributing to $F_1(Q^2)$ and those contributing to $F_2(\omega)$ have a one-to-one correspondence. Moreover, the contributions from corresponding diagrams satisfy the Drell-Yan[6] relation. This can be checked by using a simple power-counting method. Take any diagram contributing to $F_1(Q^2)$. First we have to identify the wee and the nonwee particles in the intermediate state. Since only the electromagnetically scattered parton is nonwee, this identification is trivial once we can lump all strong vertices either in the initial undressing or in the final redressing of the physical proton. Then the origin of the various powers of $q_\perp$ in the $q_\perp \to \infty$ limit can be traced following the second paper in Ref. 3. One obtains a factor of $q_\perp$ from each internal wee line-particle line, a factor of $q_\perp^{-1}$ from each loop containing a wee-particle line, a factor of $\sqrt{q_\perp}$ from each meson-baryon vertex where *only one* of the two baryons is wee and a factor of $q_\perp^{-1}$ from each wee-particle-containing energy denominator. Thus, for example, the contribution from Fig. 7(a) is proportional to $q_\perp^{-2}$ and that from Fig. 7(b) to $q_\perp^{-3}$. The corresponding diagrams for $F_2(\omega)$ are shown in Figs. 8(a) and 8(b) and in the $\omega \to 1$ limit their contributions are proportional to $\omega^{-1}(1-\omega^{-1})$ and $\omega^{-1}(1-\omega^{-1})^2$, respectively, in agreement with the Drell-Yan relation.

We conclude this review with one observation. It was suggested in Sec. III that in the parton picture all hadronic electromagnetic form factors should fall off with the same power of $q_\perp^{-1}$ as $q_\perp \to \infty$. In terms of the diagrams of the above model, this would be the case provided to every diagram for the form factor of a baryon, there is a corresponding diagram (with the same wee particles) for the meson form factor giving the same leading $q_\perp$ dependence as $q_\perp \to \infty$. This correspondence is generally true and is elegantly exemplified in Figs. 9(a) and 9(b) where each contribution is proportional to $q_\perp^{-1}$ for large $q_\perp$. However, there are some situations when the diagram for one case happens to vanish owing to a symmetry principle, but does not vanish for the other case. In particular, this occurs when all the wee particles are an odd number of pions in which case their contribution to the pion (but not the nucleon) form factor vanishes (cf. Fig. 10). In order to have universality in the asymptotic behavior of all electromagnetic form factors, one has to make the necessary but *ad hoc* additional assumption that this small subset of "anomalous" diagrams makes no difference to the final result.

V. PARTON EQUATION FOR SINGLE-PARTICLE ELECTROPRODUCTION

Starting with the amplitude $\langle p_B, p_A | J_\mu | p \rangle$ in the $Q^2 = q_\perp^2 \to \infty$ limit, we shall now set up and consider the basic equation of our model. Although this matrix element has well-defined external spin factors, we are in fact interested in

$$\sum_{\text{spins}} \langle p | J_\mu | p_A, p_B \rangle \langle p_B, p_A | J_\nu | p \rangle$$

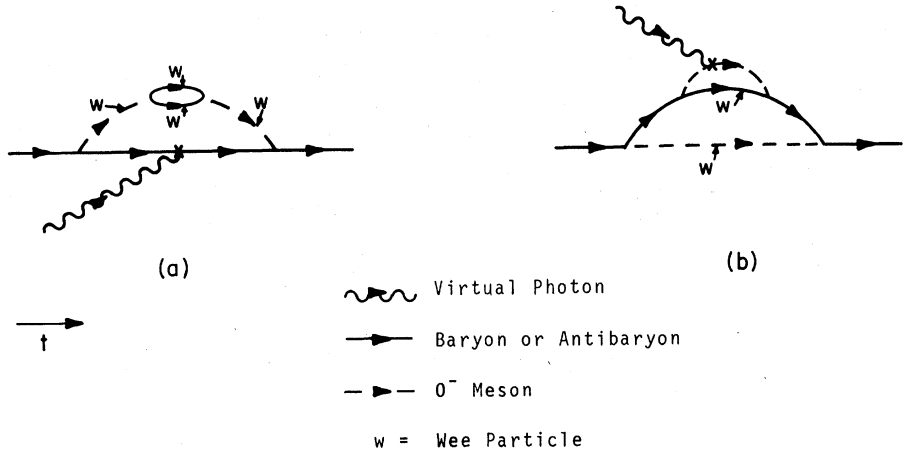

FIG. 7. Two time-ordered diagrams contributing to $F_1(Q^2)$ in the DLY model: (a) contribution $\propto q_\perp^{-2}$, (b) contribution $\propto q_\perp^{-3}$.

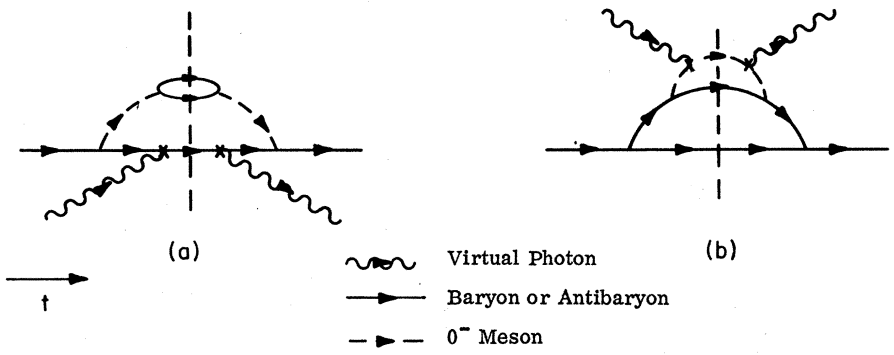

FIG. 8. Two diagrams (corresponding to Fig. 7) contributing to $F_2(\omega)$: (a) contribution $\propto\omega^{-1}(1-\omega^{-1})$, (b) contribution $\propto\omega^{-1}(1-\omega^{-1})^2$.

[see Eq. (2.5)] wherein these have disappeared. These external spin factors do not play any role in determining the leading $q_\perp$ dependence of the above spin-summed quantity when $q_\perp \to \infty$ (this will become clearer later). Hence, for notational brevity, we shall always absorb them in the appropriate vertex functions.

Let us, for simplicity, begin with the situation illustrated in Fig. 4. This was discussed in Sec. III in connection with the derivation of kinematic restrictions enforced by parton dynamics. Undressing the current J^μ by $U^{-1}j^\mu U$ ($\mu=0,3$), we note that the bare current j_μ acts as a one-body operator in scattering a single charged constituent a and giving it the momentum $\vec{p}_s$ as defined in Eq. (3.2). Now let l_α and l_β denote two distinct subsets of states standing for l_α partons in the bunch α and for l_β partons in the bunch β, respectively (see discussion in Sec. III). Introducing a complete set of such states and summing over them, we can use the factorization[15] of the U matrix in our model and write

$$\langle p_A, p_B | U^{-1} j^\mu | Up\rangle = \sum_a \sum_{l_\alpha, l_\beta} \langle p_B | U^{-1} | l_\beta, l_\alpha\rangle \langle p_A, l_\alpha | U^{-1} | a, p_s\rangle \langle l_\beta + a, p_s | j^\mu | Up\rangle . \tag{5.1}$$

Because of Eqs. (4.2) and (4.6), we have[16]

$$\langle l_\beta + a, p_s | j^{0,3} | Up\rangle = \frac{\lambda_a f_p^{l_\beta}(\vec{p}_s - \vec{q}_\perp; \vec{p}_1^{\,\beta}, \ldots, \vec{p}_l^{\,\beta})}{(2\pi)^3 (P^{l_\beta})^{1/2}} , \tag{5.2}$$

where $\vec{p}_j^{\,\beta}$ is the momentum of the jth member in the bunch β with $\sum_j^{l_\beta} \vec{p}_j^{\,\beta} = \vec{p}_\beta$ and where $f_p^{l_\beta}$ is the vertex function associated with the initial undressing of the proton into $l_\beta + 1$ partons. Similarly, in analogy with Eq. (4.2), we can write

$$\langle a, p_s | U | p_A, \alpha\rangle = \frac{\delta^{(3)}\left(\vec{p}_s - \vec{p}_A - \sum_r^{l_\alpha} \vec{p}_r^{\,\alpha}\right)}{[(X_A P)^{l_\alpha}]^{1/2}} g_{p_A}^{l_\alpha}(\vec{p}_s; \vec{p}_1^{\,\alpha}, \ldots, \vec{p}_{l_\alpha}^{\,\alpha}) \tag{5.3}$$

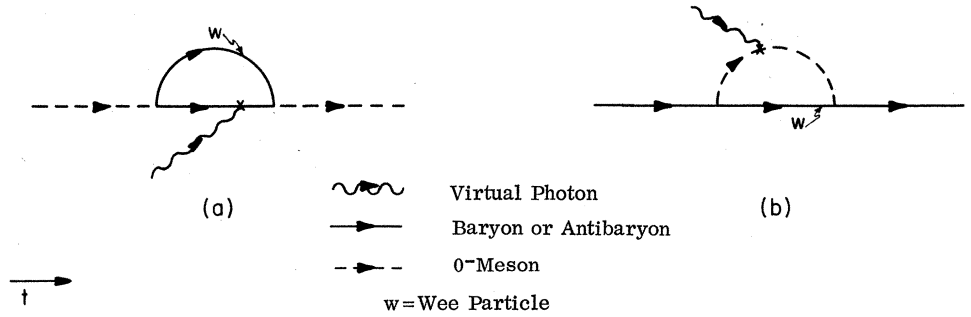

FIG. 9. Diagrams in the DLY model involving the same "wee" particle: (a) meson form factor $\propto q_\perp^{-1}$, (b) baryon form factor $\propto q_\perp^{-1}$.

and

$$\langle l_\alpha, l_\beta | U | p_B \rangle = \frac{\delta^{(3)}\left(\sum_j^{l_\beta} \vec{p}_j^{\,\beta} + \sum_r^{l_\alpha} \vec{p}_r^{\,\alpha} - \vec{p}_B\right)}{[(X_B P)^{l_\alpha + l_\beta - 1}]^{1/2}} h_{p_B}^{l_\beta, l_\alpha}(\vec{p}_1^{\,\beta}, \ldots, \vec{p}_{l_\beta}^{\,\beta}; \vec{p}_1^{\,\alpha}, \ldots, \vec{p}_{l_\alpha}^{\,\alpha}) . \tag{5.4}$$

In Eqs. (5.3) and (5.4) $\vec{p}_r^{\,\alpha}$ is the momentum of the rth member in the bunch α and $\sum_r^{l_\alpha} \vec{p}_r^{\,\alpha} = \vec{p}_\alpha$. Moreover, $h_{p_B}^{l_\beta, l_\alpha}$ and $g_{p_A}^{l_\alpha}$ are vertex functions associated respectively with the undressing of B into two bunches α, β and of A into the bunch α and the parton a carrying momentum $\vec{p}_s$. Using Eqs. (5.2), (5.3), and (5.4) in Eq. (5.1), we can write

$$\langle p_A, p_B | U^{-1} j^\mu | Up \rangle = \sum_a \sum_{l_\alpha=1}^{\infty} \sum_{l_\beta=1}^{\infty} \langle p_A, p_B | U^{-1} j^\mu | Up \rangle_{l_\alpha, l_\beta}^a , \tag{5.5}$$

where

$$\langle p_A, p_B | U^{-1} j^{0,3} | Up \rangle_{l_\alpha, l_\beta}^a = \frac{\lambda_a}{(X_B^{\,l_\alpha + l_\beta - 1} X_A^{\,l_\alpha} P^{2l_\alpha + 2l_\beta - 1})^{1/2}}$$

$$\times \prod_{j=1}^{l_\beta} \prod_{r=1}^{l_\alpha} \int d^3 p_j^\beta d^3 p_r^\alpha d^3 p_s \delta^{(3)}\left(\sum_j^{l_\beta} \vec{p}_j^{\,\beta} + \sum_r^{l_\alpha} \vec{p}_r^{\,\alpha} - \vec{p}_B\right) \delta^{(3)}\left(\vec{p}_s - \vec{p}_A - \sum_r^{l_\alpha} \vec{p}_r^{\,\alpha}\right) f_p^{l_\beta} g_{p_A}^{l_\alpha *} h_{p_B}^{l_\beta, l_\alpha *} , \tag{5.6}$$

and $f_p^{l_\beta}$, $g_{p_A}^{l_\alpha}$, and $h_{p_B}^{l_\beta, l_\alpha}$ are as defined in Eqs. (5.2), (5.3), and (5.4), respectively.

We now substitute

$$\vec{p}_r^{\,\alpha} = (1 - \chi) y_r \vec{p}_s - \vec{p}_r' \tag{5.7a}$$

and

$$\vec{p}_j^{\,\beta} = (1 - \eta_a) x_j \vec{P} + \vec{k}_{j\perp} , \tag{5.7b}$$

where $\vec{p}_s = \eta_a \vec{P} + \vec{k}_{a\perp} + \vec{q}_\perp$, $\sum_r^{l_\alpha} y_r = 1$, $\sum_r \vec{p}_r' = \vec{p}'$, $\sum_j^{l_\beta} x_j = 1$, and $\sum_j \vec{k}_{j\perp} = -\vec{k}_{a\perp}$. Thus we preserve $\sum_r \vec{p}_r^{\,\alpha} = \vec{p}^{\,\alpha}$ and $\sum_j \vec{p}_j^{\,\beta} = \vec{p}^{\,\beta}$, where $\vec{p}^{\,\alpha, \beta}$ are given by Eqs. (3.6). With this substitution and because of Eq. (2.10a), Eq. (5.6) becomes

$$\langle p_A, p_B | U^{-1} j^{0,3} | Up \rangle_{l_\alpha, l_\beta}^a = \frac{\lambda_a}{\sqrt{P}} \frac{1}{[X_A^{\,l_\alpha} (1 - X_A)^{l_\alpha + l_\beta - 1}]^{1/2}} \int_0^1 d\eta_a \int d^2 k_{a\perp} (1 - \eta_a)^{l_\beta - 1} (1 - \chi)^{l_\alpha - 1} \eta_a^{\,l_\alpha - 1}$$

$$\times \prod_j^{l_\beta - 1} \prod_r^{l_\alpha - 1} \int_0^1 dx_j \int d^2 k_{j\perp} \int_0^1 dy_r \int d^2 p_r' \theta\left(1 - \sum_j^{l_\beta - 1} x_j\right) \theta\left(1 - \sum_r^{l_\alpha - 1} y_r\right) f_p^{l_\beta} g_{p_A}^{l_\alpha *} h_{p_B}^{l_\beta, l_\alpha *} . \tag{5.8}$$

In Eq. (5.7) $f_p^{l_\beta}$, $g_{p_A}^{l_\alpha}$, and $h_{p_B}^{l_\beta, l_\alpha}$ can be written as functions of longitudinal and transverse variables defined with respect to $\vec{p}$, $\vec{p}_A$, and $\vec{p}_B$, respectively, i.e.,

$$f_p^{l_\beta} \equiv f_p^{l_\beta}(\eta_a, (1 - \eta_a) x_j; \ldots) ,$$

$$g_{p_A}^{l_\alpha} \equiv g_{p_A}^{l_\alpha}\left(\frac{1}{\chi} \frac{1 - \chi}{\chi} y_r; \ldots\right) , \tag{5.9}$$

$$h_{p_B}^{l_\beta, l_\alpha} \equiv h_{p_B}^{l_\beta, l_\alpha}\left(\frac{1 - \eta_a}{1 - \chi\eta_a} x_j, \frac{1 - \chi}{1 - \chi\eta_a} \eta_a y_r; \ldots\right) ,$$

with r (j) running from 1 to $l_\alpha - 1$ ($l_\beta - 1$) and ... standing for finite transverse variables (integrated within the finite transverse-momentum cutoff[10]) with which we shall not be concerned.

Equation (5.7), derived above for the situation depicted in Fig. 4, is the basic equation of our parton model and we shall investigate the fixed-ω and the fixed-τ_A limits with this. Let us now consider these limits in the context of this equation:

(1) Fixed-ω limit (Fig. 5, case 1, Sec. III). The general situation in this case is slightly more com-

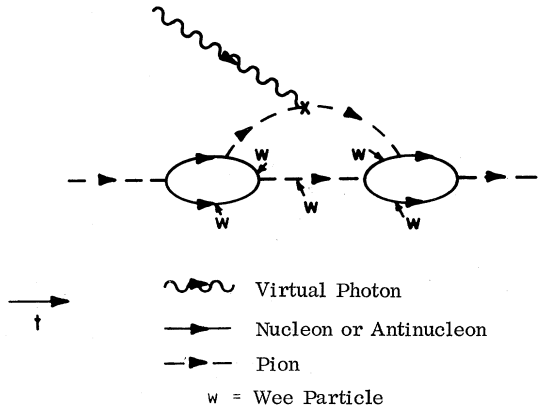

FIG. 10. A particular time-ordered diagram for the pion form factor whose contribution $\propto q_\perp^{-2}$ but where the constant of proportionality has to vanish because of G-parity invariance.

plicated than that shown in Fig. 4. However, an equation analogous to Eq. (5.8) can be written down[15] provided we extend $g^{l_\alpha}_{p_A}$, the vertex function associated with the A vertex, to include wee partons moving from the B vertex to it and take $\chi_1\chi_2=\chi$ and $\vec{p}_1'-\vec{p}_2'=\vec{p}'$ (see Sec. III). The l_α partons in the bunch α are all wee now whereas the l_β partons in the bunch β are nonwee. Since $\chi_{1,2}\sim 1\pm\mu_{1,2}q_\perp^{-1}$ and $\eta_a\sim\omega^{-1}$ in the present limit, Eq. (5.7a) – giving the momentum of the rth member in the wee bunch α – now becomes

$$\vec{p}^{\,\alpha}_{r_{1,2}}\simeq\mu_{1,2}q_\perp^{-1}y_{r_{1,2}}(\omega^{-1}\vec{P}+\vec{k}_{a\perp}+\vec{q}_\perp)-\vec{p}'_{r_{1,2}}. \tag{5.10}$$

In Eq. (5.10), the subscripts 1,2 keep track of whether the wee parton moves from the A vertex to the B vertex or vice versa (see Case 1, Sec. III) and $\sum_r y_{r_{1,2}}=1$, $\sum_r\vec{p}'_{r_{1,2}}=\vec{p}'_{1,2}$. Moreover, Eq. (5.7b) for the momentum of the jth member of the nonwee bunch β becomes

$$\vec{p}^{\,\beta}_j\simeq(1-\omega^{-1})x_j\vec{P}+\vec{k}_{j\perp}. \tag{5.11}$$

Finally, in the η_a integration we can substitute

$$\eta_a=\omega^{-1}[1-(\mu_2-\mu_1)q_\perp^{-1}z_a]^{-1},$$

so that as $q_\perp\to\infty$, $\eta_a\to\omega^{-1}$ as required by Eq. (3.12); on the other hand, in the $q_\perp\to\infty$ limit we can write

$$\int_0^1 d\eta_a\simeq\omega^{-1}(\mu_2-\mu_1)q_\perp^{-1}\int_0^{\text{finite}}dz_a$$

and replace η_a by ω^{-1} everywhere in the integrand.

We now replace X_A by ω^{-1} in accordance with Eq. (3.12). Using the equations and the substitutions of the above paragraph, we can rewrite Eq. (5.8) as

$$\begin{aligned}
&\lim_{\text{Bj}}\langle p_A,p_B|U^{-1}j^{0,3}|Up\rangle^a_{l_\alpha,l_\beta}\\
&=\frac{\lambda_a}{\sqrt{P}}\frac{1}{[\omega^{-l_\alpha}(1-\omega^{-1})^{l_\alpha+l_\beta-1}]^{1/2}}\frac{\mu_2-\mu_1}{\omega q_\perp}\int_0^{\text{fin}}dz_a\int d^2k_{a\perp}(1-\omega^{-1})^{l_\beta-1}\omega^{-l_\alpha+1}\left(\frac{\mu_{1,2}z_a}{q_\perp}\right)^{l_\alpha-1}\\
&\quad\times\prod_j^{l_\beta-1}\prod_r^{l_\alpha-1}\int_0^1 dx_j\theta\Big(1-\sum_j^{l_\beta-1}x_j\Big)\int d^2k_{j\perp}\int_0^1 dy_{r_{1,2}}\theta\Big(2-\sum_r^{l_\alpha-1}y_{r_{1,2}}\Big)\int d^2p'_{r_{1,2}}g^{l_\alpha *}_{p_A}h^{l_\beta,l_\alpha *}_{p_B}f^{l_\beta}_p\\
&=\frac{\lambda_a}{\sqrt{P}}\left(\frac{(1-\omega^{-1})^{l_\beta-l_\alpha-1}}{\omega^{l_\alpha}}\right)^{1/2}\left(\frac{\mu}{q_\perp}\right)^{l_\alpha}\int_0^{\text{fin}}dz_a\int d^2k_{a\perp}\prod_j^{l_\beta-1}\prod_r^{l_\alpha-1}z_a^{l_\alpha-1}\\
&\quad\times\int_0^1 dx_j\theta\Big(1-\sum_j^{l_\beta-1}x_j\Big)\int d^2k_{j\perp}\int_0^1 dy_{r_{1,2}}\theta\Big(2-\sum_r^{l_\alpha-1}y_{r_{1,2}}\Big)\int d^2p'_{r_{1,2}}g^{l_\alpha *}_{p_A}h^{l_\beta,l_\alpha *}_{p_B}f^{l_\beta}_p.
\end{aligned} \tag{5.12}$$

Equation (5.12) is the fundamental equation which will give us information on the single-particle electroproduction amplitude in the fixed-ω limit. Here $\mu\sim\mu_{1,2}$ and from Eq. (5.9) we have

$$\begin{aligned}
&f^{l_\beta}_p\equiv f^{l_\beta}_p(\omega^{-1},(1-\omega^{-1})x_j;\ldots),\\
&g^{l_\alpha}_{p_A}\equiv g^{l_\alpha}_{p_A}\Big(1,\frac{\mu_{1,2}}{q_\perp}y_{r_{1,2}};\ldots\Big),\\
&h^{l_\beta,l_\alpha}_{p_B}\equiv h^{l_\beta,l_\alpha}_{p_B}\Big(x_j,\frac{\omega}{\omega-1}\frac{\mu_{1,2}}{q_\perp}y_{r_{1,2}};\ldots\Big).
\end{aligned} \tag{5.13}$$

The functional dependence shown in Eq. (5.13) is a direct consequence of the fact that the bunch β is nonwee in this case whereas the bunch α consists exclusively of wee partons.

(2) Fixed-τ_A limit (Fig. 6, case 2, Sec. III). In this case we can use Eq. (5.8) directly with the constraints that $\eta_a\sim 1-mq_\perp^{-1}$ and $X_A\simeq\chi\simeq\tau_A$. Hence

$$\begin{aligned}
&\vec{p}^{\,\alpha}_r\simeq(1-\tau_A)y_r\eta_a\vec{P}+(1-\tau_A)y_r\vec{q}_\perp+\text{finite}\\
&\text{and}\\
&\vec{p}^{\,\beta}_j\simeq mq_\perp^{-1}x_j\vec{P}+\vec{k}_{j\perp}.
\end{aligned} \tag{5.14}$$

Now in the η_a integration we substitute

$$\eta_a = 1 - m' w_a / q_\perp ,$$

where $m' \sim m$ so that since $\eta_a \to 1$ as $q_\perp \to \infty$, we can take

$$\int_0^1 d\eta_a \sim \frac{m}{q_\perp} \int_0^{\text{fin}} dw_a$$

and replace η_a by 1 everywhere in the integrand. With these changes, Eq. (5.8) becomes

$$\begin{aligned}\lim_{\tau_A} \langle p_A, p_B | U^{-1} j^{0,3} | Up \rangle^a_{l_\alpha, l_\beta} &= \frac{\lambda_a}{\sqrt{P}} \frac{1}{[\tau_A{}^{l_\alpha}(1-\tau_A)^{l_\alpha + l_\beta - 1}]^{1/2}} \frac{m}{q_\perp} \int_0^{\text{fin}} dw_a \int d^2 k_{a\perp} \left(\frac{m w_a}{q_\perp}\right)^{l_\beta - 1} (1-\tau_A)^{l_\alpha - 1} \\ &\times \prod_j^{l_\beta - 1} \prod_r^{l_\alpha - 1} \int_0^1 dx_j \theta\left(1 - \sum_j^{l_\beta - 1} x_j\right) \int d^2 k_{j\perp} \int_0^1 dy_r \theta\left(1 - \sum_r^{l_\alpha - 1} y_r\right) \int d^2 p'_r g^{l_\alpha *}_{p_A} h^{l_\beta, l_\alpha *}_{p_B} f^{l_\beta}_{p} \\ &= \frac{\lambda_a}{\sqrt{P}} \left[\frac{(1-\tau_A)^{l_\alpha - l_\beta - 1}}{\tau_A{}^{l_\alpha}}\right]^{1/2} \left(\frac{m}{q_\perp}\right)^{l_\beta} \int_0^{\text{fin}} dw_a \int d^2 k_{a\perp} \\ &\times \prod_j^{l_\beta - 1} \prod_r^{l_\alpha - 1} w_a{}^{l_\beta - 1} \int_0^1 dx_j \theta\left(1 - \sum_j^{l_\beta - 1} x_j\right) \int d^2 k_{j\perp} \int_0^1 dy_r \theta\left(1 - \sum_r^{l_\alpha - 1} y_r\right) \int d^2 p'_r g^{l_\alpha *}_{p_A} h^{l_\beta, l_\alpha *}_{p_B} f^{l_\beta}_{p} .\end{aligned} \tag{5.15}$$

Here,

$$\begin{aligned} f^{l_\beta}_{p} &\equiv f^{l_\beta}_{p}\left(1, \frac{m}{q_\perp} x_j; \ldots\right), \\ g^{l_\alpha}_{p_A} &\equiv g^{l_\alpha}_{p_A}(\tau_A{}^{-1}, (\tau_A{}^{-1} - 1) y_r; \ldots), \\ h^{l_\beta, l_\alpha}_{p_B} &\equiv h^{l_\beta, l_\alpha}_{p_B}\left(\frac{m}{q_\perp} \frac{x_j}{1-\tau_A}, y_r; \ldots\right). \end{aligned} \tag{5.16}$$

Equation (5.15) is our basic equation for the fixed-τ_A limit. The functional dependence shown in Eq. (5.16) reflects the wee (nonwee) nature of the bunch $\beta(\alpha)$ in this case.

VI. ROLE OF WEE PARTONS IN THE FIXED-ω AND FIXED-τ_A LIMITS

We first write the equations [corresponding to Eq. (4.8)] for the elastic electromagnetic form factors[17] of the particles A, B, and p. Assigning the momenta $\vec{p}_A$, $\vec{p}_B$, and $\vec{p}_p = \vec{p}$, respectively, to A, B, and p before they are scattered elastically by a virtual photon of momentum $\vec{q}_\perp$ in the infinite-momentum frame and considering the contribution from a certain configuration of l wee partons, we have

$$\begin{aligned}\lim_{q_\perp \to \infty} F^a_{l_K} &= \lambda_a \left(\frac{\mu}{q_\perp}\right)^l \int_0^{\text{fin}} dz_a \int d^2 k_{a\perp} \\ &\times \prod_{j \neq a}^{l-1} \int_0^1 dx_j \int d^2 k_{j\perp} \theta\left(1 - \sum_{j \neq a}^{l-1} x_j\right) f^{l *}_{p'_K} f^{l}_{p_K} .\end{aligned} \tag{6.1}$$

In Eq. (6.1) the subscript K can be A, B, or p. Here $f^l_{p'_K}$ and $f^l_{p_K}$ have the same longitudinal variables 1, $\mu x_j q_\perp{}^{-1}$ – only their finite transverse variables are different by finite amounts and these are immaterial. Hence, for the purpose of determining the leading $q_\perp$ dependence, $f^l_{p'_K}$ can be taken to behave in the same was as $f^l_{p_K}$. Now a comparison between Eq. (6.1) and Eqs. (5.12)–(5.15) clearly brings out the role of the exchanged wee partons in controlling the leading $q_\perp$ dependence in the latter cases. We consider the two relevant asymptotic limits separately.

(1) Fixed-ω limit. In this case it will be convenient to consider Eq. (6.1) with $l = l_\alpha$. Hence in the above equation, as in Eq. (5.12) (Fig. 5), l_α is the number of wee partons being exchanged. In either equation there appears a factor of $(\mu q_\perp{}^{-1})^{l_\alpha}$ outside the integrals. The $q_\perp$ dependences in the integrands come from the longitudinal variables in $g^{l_\alpha}_{p_A}$, $h^{l_\beta, l_\alpha}_{p_B}$ [see Eq. (5.13)] and from those in $f^{l_\alpha}_{p_K}$. It is to be noted that the vertex functions $g^{l_\alpha}_{p_A}$ and $f^{l_\alpha}_{p_A}$ are very similar in that they involve transitions of the same physical particle with the same momentum into one particular nonwee parton and a certain bunch of l_α wee partons. The only difference between these functions lies in the fact that the former involves a vertex where some of the wee partons are emitted and some absorbed, whereas the latter involves one where all are emitted. *But because of their soft longitudinal components of momenta in the $P \to \infty$ frame, the wee*

partons are unable to distinguish between emission and absorption in the $q_\perp \to \infty$ limit. More precisely, in the model of Ref. 3, to every order there is a one-to-one correspondence between $f^{l\alpha}_{p_A}$ and $g^{l\alpha}_{p_A}$ and, as $q_\perp \to \infty$, the dominant power of $q_\perp^{-1}$ is the same for vertices belonging to each corresponding pair (specific examples will be found in Appendix A). Hence we shall assume that the leading behavior of these two vertex functions are the same in the large-$q_\perp$ limit.

Arguments will now be given in favor of assuming a similar relation between $h^{l_\beta,l\alpha}_{p_B}$ and $f^{l\alpha}_{p_B}$. These involve vertices undressing the same physical particle B and the same wee partons. The difference is that $h^{l_\beta,l\alpha}_{p_B}$ has l_β associated nonwee partons whereas $f^{l\alpha}_{p_B}$ has only one (i.e., $f^{l\alpha}_{p_B}$ is similar to $h^{1,l\alpha}_{p_B}$). But the wee partons – which generate the crucial factor determining the dominant $q_\perp$ behavior in the large-$q_\perp$ limit – are precisely the same for either. Counting on this fact, we shall assume that the number of associated nonwee partons has nothing to do with the dominant $q_\perp$ behavior of a vertex so that $h^{l_\beta,l\alpha}_{p_B}$ and $f^{l\alpha}_{p_A}$ give the same leading power of $q_\perp^{-1}$ as $q_\perp \to \infty$. In the model of Ref. 3, there is no longer a one-to-one correspondence between $h^{l_\beta,l\alpha}_{p_B}$ and $f^{l\alpha}_{p_B}$ so that an order-by-order comparison is not possible any more. For each perturbative vertex contributing to $f^{l\alpha}_{p_B}$, there is now a class of vertices (involving the same wee partons) for $h^{l_\beta,l\alpha}_{p_B}$ arising out of l_β (≥ 1) nonwee partons in the latter. However, when $q_\perp \to \infty$, the leading $q_\perp$ dependence of this class is invariably[18] the same (although some particular vertices of the above-mentioned class may not contribute to this leading behavior) as that of the corresponding vertex for $f^{l\alpha}_{p_B}$ (specific examples will be found in Appendix B). This suggests that our ansatz on the dominant power of $q_\perp^{-1}$ in $h^{l_\beta,l\alpha}_{p_B}$ and $f^{l_\beta}_{p_B}$ being the same in the large-$q_\perp$ limit is reasonable.

The above assumptions, although strong, appear to be sensible from a physical standpoint. Arguments for their justification can be given in the model of Ref. 3 based on old-fashioned diagram calculations. Given these assumptions, a comparison of Eq. (6.1) (with $l = l_\alpha$) with Eq. (5.12) implies that

$$\lim_{\text{Bj}} \sum_{l_\beta} \langle p_A, p_B | U^{-1} j^{0,3} | Up \rangle^a_{l,l_\beta} \propto \left(\frac{F^a_{l_A}(Q^2) F^a_{l_B}(Q^2)}{P} \right)^{1/2} . \tag{6.2}$$

In Eq. (6.2) the left-hand side has been summed over the irrelevant nonwee partons and the proportionality constant includes inconsequential spin factors and an unknown function of ω. From this equation we shall infer – in the manner of Drell and Yan[6] (see Sec. IV) – that

$$\lim_{\text{Bj}} \langle p_A, p_B | U^{-1} j^{0,3} | Up \rangle \propto \left(\frac{F_A(Q^2) F_B(Q^2)}{P} \right)^{1/2} . \tag{6.3}$$

Equation (6.3) can be rewritten in terms of the spin-summed square of the matrix element as

$$\lim_{\text{Bj}} \overline{\sum_{\text{spins}}} (2\pi)^9 \langle Up | j^{0,3} U | p_A, p_B \rangle \langle p_B, p_A | U^{-1} j^{0,3} | Up \rangle = \frac{F_A(Q^2) F_B(Q^2)}{P} u(\omega) , \tag{6.4}$$

where $u(\omega)$ is an unknown function of ω.

(2) Fixed-τ_A limit. In this case it is convenient to choose $l = l_\beta$ in Eq. (6.1) so that the number of wee partons being exchanged here is now the same as in Eq. (5.15) (Fig. 6), i.e., l_β. The other considerations proceed as in the fixed-ω limit. In both equations we have an over-all factor of $(\mu q_\perp^{-1})^{l_\beta}$. The $q_\perp$ dependence in the integrand of Eq. (5.15) comes from the vertex functions $f^{l_\beta}_p$ and $h^{l_\beta,l\alpha}_{p_B}$ [see Eq. (5.16)]. The former occurs explicitly in Eq. (6.1) for $K = p$. The latter is assumed, using the same argument[18] as given above, to have the same dominant $q_\perp$ behavior in the large-$q_\perp$ limit as $f^{l_\beta}_{p_B}$. With this assumption, the equation analogous to Eq. (6.3) for this case is

$$\lim_{\tau_A} \langle p_A, p_B | U^{-1} j^{0,3} | Up \rangle \propto \left(\frac{F_p(Q^2) F_B(Q^2)}{P} \right)^{1/2} , \tag{6.5}$$

and that corresponding to Eq. (6.4) is

$$\lim_{\tau_A} \overline{\sum_{\text{spins}}} (2\pi)^9 \langle Up | j^{0,3} U | p_A, p_B \rangle \langle p_B, p_A | U^{-1} j^{0,3} | Up \rangle = \frac{F_p(Q^2) F_B(Q^2)}{P} v(\tau_A) , \tag{6.6}$$

$v(\tau_A)$ being an unknown function of τ_A.

The meaning of Eqs. (6.3) and (6.5) in old-fashioned perturbation theory can be understood in the following way. Consider Eq. (6.3) first. Take any two time-ordered diagrams contributing to $F_A(Q^2)$, $F_B(Q^2)$ that involve the emission and reabsorption of a certain bunch of l_α wee partons. There will be a class of diagrams with the same wee partons exchanged for the process $ep \to e'AB$ in the fixed-ω limit, the number in the class depending on the number l_β of nonwee partons untouched by the virtual photon. However, when $q_\perp \to \infty$, the leading $q_\perp$ dependence[19] in the latter class of diagrams in the fixed-ω limit will be related to the dominant $q_\perp$ behavior of the former by Eq. (6.4).[20] One example[21] with $l_\alpha = 1$ and $l_\beta = 2$ is illustrated in Fig. 11 and should be compared with the form-

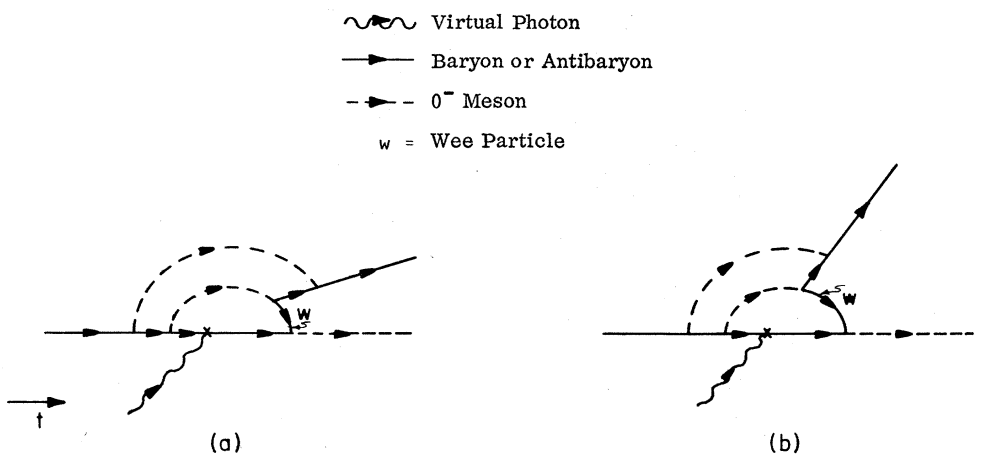

FIG. 11. Specific diagrams for the meson electroproduction amplitude: (a) leading contribution $\propto q_\perp^{-1}$, (b) nonleading contribution $\propto q_\perp^{-2}$.

factor cases shown in Fig. 9. Similarly, for the fixed-τ_A limit, the dominant $q_\perp$ behavior of any two diagrams for $F_p(Q^2)$ and $F_B(Q^2)$ involving the same bunch of l_β wee partons will be related to the leading $q_\perp$ dependence of the corresponding class of diagrams for the amplitude of $ep \to e'AB$ by Eq. (6.5).

VII. ASYMPTOTIC BEHAVIOR OF $\mathcal{W}_2$

We shall now convert Eqs. (6.4) and (6.6) into forms that are more directly related to experiment. Consider first the fixed-ω limit. If we take $\mu, \nu = 0, 3$ in Eq. (2.5) and apply the $P \to \infty$ limit to both sides of this equation using Eqs. (2.7) and (2.8), we obtain that in the infinite-momentum frame,

$$\lim_{\text{Bj}} \mathcal{W}_2 \frac{P^2}{M_p^2} = \frac{P^2}{M_p} \int_0^1 dX_A \int d^2k_{A\perp}\, \delta\left(\kappa_A - \frac{X_A M_p}{2} - \frac{M_A^2 + k_{A\perp}^2}{2X_A M_p}\right) \delta\left(\frac{2M_p\nu}{2P} - \frac{Q^2}{2X_A P}\right)$$
$$\times (2\pi)^6 \overline{\sum_{\text{spins}}} \langle p | J^{0,3} | p_A, p_B, \rangle \langle p_A, p_B | J^{0,3} | p \rangle . \tag{7.1}$$

In the right-hand side of Eq. (7.1), we have used Eqs. (2.9), (2.10c), and (3.8). Now we substitute Eq. (6.4) in Eq. (7.1) to obtain

$$\lim_{\text{Bj}} \mathcal{W}_2 \frac{P^2}{M_p^2} = \frac{P^2}{M_p} \int_0^1 dX_A\, \delta\left(X_A - \frac{Q^2}{2M_p\nu}\right) 2X_A^2$$
$$\times \frac{P}{Q^2} \int \pi dk_{A\perp}^2\, \delta(2X_A\kappa_A M_p - X_A^2 M_p^2 - M_A^2 - k_{A\perp}^2) 2X_A M_p \left(\frac{1}{2\pi}\right)^3 \frac{1}{P} F_A(Q^2) F_B(Q^2) u(\omega),$$

or

$$\lim_{\text{Bj}} \nu \mathcal{W}_2 = F_A(Q^2) F_B(Q^2) U(\omega), \tag{7.2}$$

where $U(\omega) = u(\omega) M_p/(2\pi\omega)^2$ is an unknown function of ω.

A similar analysis can be made for the fixed-τ_A limit. We write Eq. (2.5) as

$$\mathcal{W}_2 \frac{P^2}{M_p^2} = \frac{P^2}{M_p} \int_0^1 dX_A \int \pi dk_{A\perp}^2\, \delta\left(\kappa_A - \frac{X_A M_p}{2} - \frac{M_A^2 + k_{A\perp}^2}{2X_A M_p}\right) 2P\delta\left(M_p^2 + 2M_p\nu - \frac{k_{A\perp}^2 + M_A^2}{X_A} - \frac{(\vec{q}_\perp - \vec{k}_{A\perp})^2 + M_B^2}{1 - X_A}\right)$$
$$\times (2\pi)^6 \overline{\sum_{\text{spins}}} \langle p | J^{0,3} | p_A, p_B \rangle \langle p_A, p_B | J^{0,3} | p \rangle . \tag{7.3}$$

Using Eqs. (3.17), (3.20), and (6.6) in Eq. (7.3), we have

$$\lim_{\tau_A} \mathcal{W}_2 \frac{P^2}{M_p^2} = \frac{P^2}{M_p} \int \pi dk_{A\perp}^2\, \delta(k_{A\perp}^2 - 2\tau_A M_p \kappa_A) 2M_p \tau_A 2p$$
$$\times \int_0^1 dX_A\, \delta(\tau_A - X_A) \left(\left|\frac{M_A^2}{\tau_A^2} - \frac{M_B^2}{(1-\tau_A)^2}\right|\right)^{-1} \left(\frac{1}{2\pi}\right)^3 \frac{1}{P} F_B(Q^2) F_p(Q^2) v(\tau_A),$$

or

$$\lim_{\tau_A} \mathcal{W}_2 = F_p(Q^2) F_B(Q^2) V(\tau_A), \tag{7.4}$$

where

$$V(\tau_A) = \frac{1}{2\pi^2} \frac{M_p^2 \tau_A v(\tau_A)}{\left| \frac{M_A^2}{\tau_A^2} - \frac{M_B^2}{(1-\tau_A)^2} \right|}$$

is an unknown function of τ_A.

In Sec. IV we argued that in the parton picture all electromagnetic form factors should asymptotically fall off with Q^2 with a universal power law. Adopting this view, we can rewrite Eqs. (7.2) and (7.4) by dropping the subscripts of the form factors

$$\begin{aligned} \lim_{\text{Bj}} \nu \mathcal{W}_2 &= [F(Q^2)]^2 U(\omega), \\ \lim_{\tau_A} \mathcal{W}_2 &= [F(Q^2)]^2 V(\tau_A). \end{aligned} \tag{7.5}$$

Since the structure function $\mathcal{W}_2$ is related to the azimuth-averaged differential cross section for near-forward (i.e., $\theta_e \simeq 0$) single-particle electroproduction by Eq. (2.6), Eq. (7.5) should be directly testable by experiment.

Before concluding this section we have one comment to make. Equation (6.2) is the fundamental relation that leads to the behavior of $\nu \mathcal{W}_2$ in the Bjorken limit predicted above. In deriving this equation in Sec. VI, we ignored any distinction between wee partons emitted from the B vertex before the interaction of the ath nonwee parton with the virtual photon and those emitted from the same after this interaction. One may argue that the behavior of these two cases will be different in time-ordered perturbation theory. It is easy to verify explicitly in the model of Ref. 3 that for large $q_\perp$ the leading $q_\perp$ dependence of any time-ordered graph of the first kind is the same as that of a corresponding graph (with the same wee-parton exchanges) of the second kind in the same order of the strong-coupling constant. Thus, using the power-counting technique outlined in Sec. IV and in Ref. 19, we can see that the leading $q_\perp$ dependence of Fig. 12(b) in the fixed-ω limit is the same as that of Fig. 12(a), i.e., $\propto q_\perp^{-1}$. Hence any difference between these two kinds of diagrams does not affect our conclusions. More generally, graphs of the type of Fig. 13(a) where wee partons are exchanged between the initial undressing vertex and the A vertex are covered by Eq. (6.2).

The above discussion brings out an important point. We have adopted the view, suggested by the parton picture, that all electromagnetic form factors should fall off universally at large Q^2 and $\nu \mathcal{W}_2$ or $\mathcal{W}_2$ (depending on the limit chosen) should be proportional to the square of this universal power of Q^{-2} times an unknown scale function as expressed in Eq. (6.5). With this viewpoint and in our model the leading $q_\perp$ dependence of the contribution to the asymptotic single-particle electroproduction amplitude from any parton configuration is controlled only by the number and type of wee partons being exchanged, it does not depend on the nature of the vertices they are being emitted from or absorbed in. This is why there is no difference between Fig. 13(a) and Fig. 5 so long as the wee partons are the same. In the same way in the fixed-τ_A limit Fig. 13(b) which includes wee-parton exchanges between the initial undres-

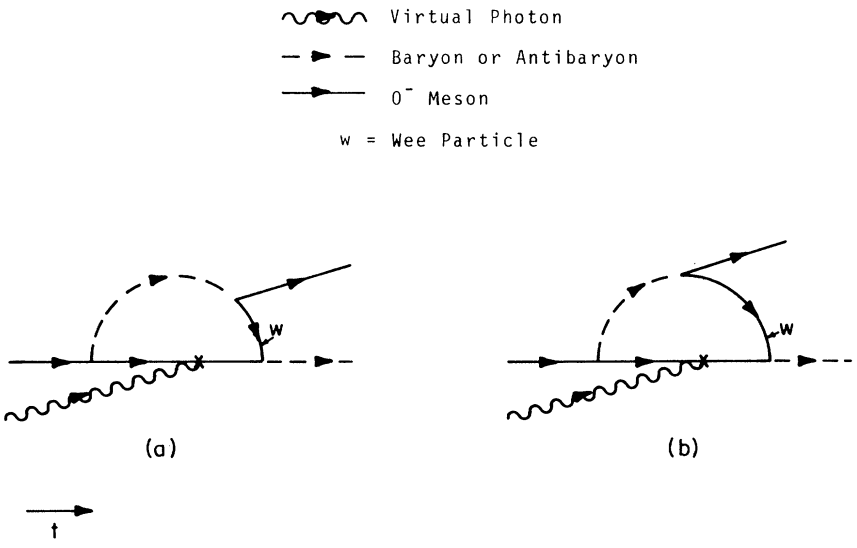

FIG. 12. Diagrams for the reaction $ep \to e'AB$ with the "wee" particle emitted (a) before and (b) after the interaction with the electromagnetic current.

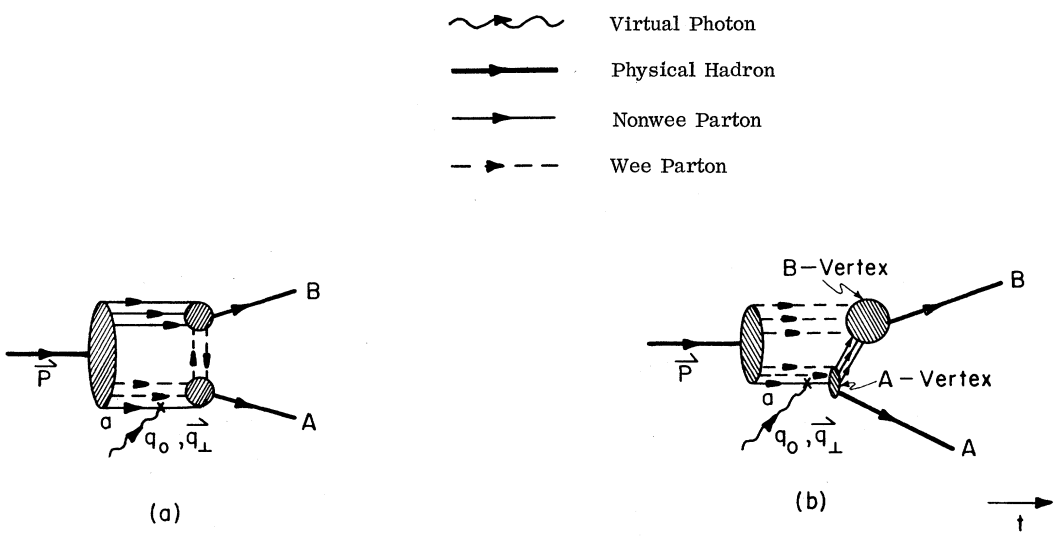

FIG. 13. Additional diagrams for the reaction $ep \to e'AB$ with wee partons exchanged between the A vertex and the initial undressing vertex: (a) fixed-ω limit, (b) fixed-τ_A limit.

sing vertex and the A vertex is covered by Eq. (6.5).

VIII. CONCLUDING REMARKS

We have two types of parton-model results for large-Q^2 single-particle electroproduction in the fixed-ω and fixed-τ_A limits. The first type is a straightforward consequence of the parton picture and consists of kinematic restrictions on the free variable in each limit, as given by Eqs. (3.12) and (3.17). In the laboratory frame this amounts to one of the final particles emerging predominantly in the direction of the virtual photon – as expressed in Eqs. (3.13) and (3.19). The second kind of predictions depend additionally on certain reasonable theoretical assumptions on appropriate vertex functions and relate the asymptotic behavior of the structure function $\mathcal{W}_2$ to the square of the asymptotic electromagnetic form factor times unknown functions of the scaling variables by means of Eq. (7.5).

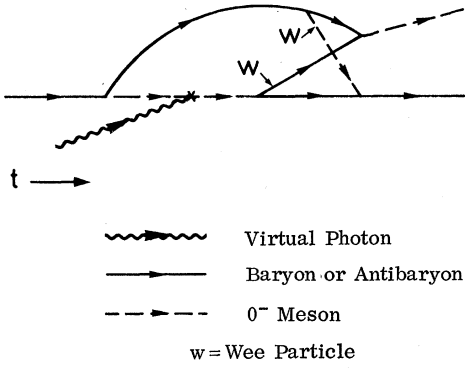

FIG. 14. Particular perturbative diagram included in Fig. 5.

Equations (3.12) and (3.17)–which should be easier to test experimentally than Eq. (7.5)–are clearly founded on stronger bases than the latter. In fact, we do not pretend that Eq. (7.5) is any more than a conjecture based on arguments that seem plausible in the parton picture. However, the basic qualitative feature of Eq. (7.5), namely that $\nu\mathcal{W}_2$ or $\mathcal{W}_2$ (depending on the limit) should tend to zero as some power of Q^{-2} is inevitable in any self-consistent parton treatment of the problem. For the specific process $ep \to en\rho^+$ a different prediction–namely, nontrivial scaling for $\nu\mathcal{W}_2$ in the Bjorken limit – has been given by Lee[22] in a model based on the current-field identity. Another result to compare is the prediction of Frishman *et al.*[23] (from light-cone-dominance assumption) that in the fixed-ω limit $\nu\mathcal{W}_2$ should behave as $Q^{-2\alpha}F_2(\omega, \tau)$, where $\tau = -(p+q-p_A)^2$ and α is related to the dimension of the leading field in the operator-product expansion. All these results will be confronted with experiment at Cornell before long.

ACKNOWLEDGMENTS

This investigation originated from a remark of Professor D. R. Yennie and was sustained by many helpful and guiding suggestions from Professor T. M. Yan, to both of whom the author expresses his gratitude.

ADDENDUM

We have recently learned from Professor R. P. Feynman that some of the above ideas have

occurred to him independently.

APPENDIX A:
COMPARISON OF $f^{l\alpha}_{p_A}$ WITH $g^{l\alpha}_{p_A}$ FOR LARGE $q_\perp$ IN THE DLY MODEL

The large-$q_\perp$ behavior of specific perturbative vertices contributing to $f^{l\alpha}_{p_A}$ and $g^{l\alpha}_{p_A}$ can be studied explicitly in the pseudoscalar field theory of Drell, Levy, and Yan[3] (DLY). Here we demonstrate with some examples that, in this model, the dominant power of $q_\perp^{-1}$ is the same for vertices with the same particles and does not depend on whether the wee ones are emitted or absorbed. For brevity, we use the power-counting technique outlined in Sec. IV, although the reader can verify our results by direct computation. The old-fashioned diagrams to be considered are displayed in Fig. 15 – in cases (a), (c), and (d) A is a baryon whereas in case (b) it is a 0^- meson. For the pair (a), we obtain a factor of $q_\perp^{-1}$ from the wee-particle-containing energy denominator and one of $\sqrt{q_\perp}$ from the normalization of the wee particle (for an internal "wee" line two such factors give $q_\perp$ – see Sec. IV); hence each vertex is proportional to $\sqrt{q_\perp^{-1}}$. For the pair (b) we have not only the same factors as above but also an additional $\sqrt{q_\perp}$ generated by only one member of the baryon-antibaryon pair being wee; hence each vertex is $q_\perp$-independent. The vertices (c) have two wee particles and two wee-particle-containing energy denominators so that each is proportional to $q_\perp^{-1}$. Each vertex of the pair (d) has one wee particle but two wee-particle-containing

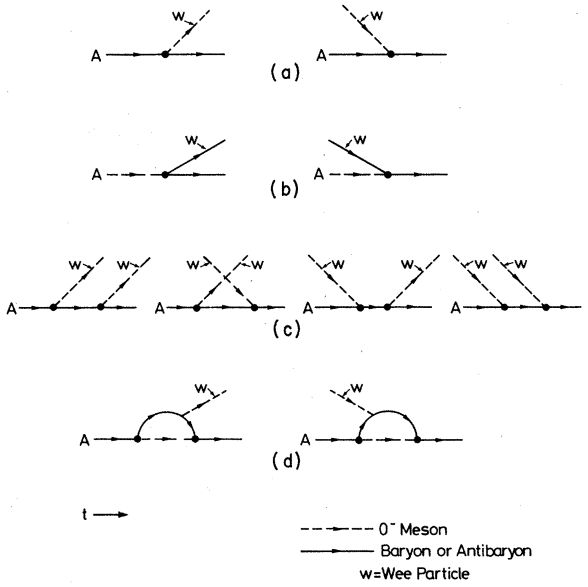

FIG. 15. Examples of corresponding vertices for $f^{l\alpha}_{p_A}$ and $g^{l\alpha}_{p_A}$ (see Appendix A).

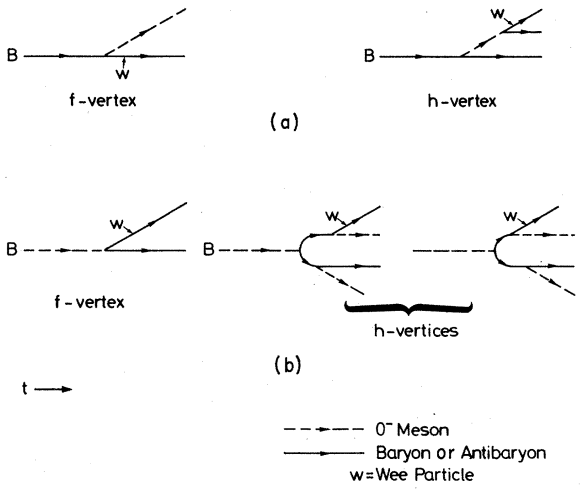

FIG. 16. Examples of corresponding vertices for $f^{l\alpha}_{p_B}$ and $h^{l\beta,\,l\alpha}_{p_B}$ (see Appendix B).

energy denominators, thereby being proportional to $\sqrt{q_\perp^{-3}}$. Clearly, "crossing" one or more wee particles has no effect on the dominant $q_\perp$ dependence of a vertex.

APPENDIX B:
LARGE-$q_\perp$ BEHAVIOR OF $f^{l\alpha}_{p_B}$ AND $h^{l\beta,l\alpha}_{p_B}$ IN THE DLY MODEL

Here also we demonstrate the validity of the claim made in Sec. V (regarding the relation between $h^{l\beta,l\alpha}_{p_B}$ and $f^{l\alpha}_{p_B}$ when $q_\perp \to \infty$) with specific perturbative examples. Figure 16 contains the relevant diagrams. First, it will be noted that the corresponding diagrams are not of the same order. In case (a) $l_\alpha = 1$, $l_\beta = 2$, B is a fermion and so is the wee particle; for the f vertex, the other non-wee particle is a meson whereas for the h vertex,

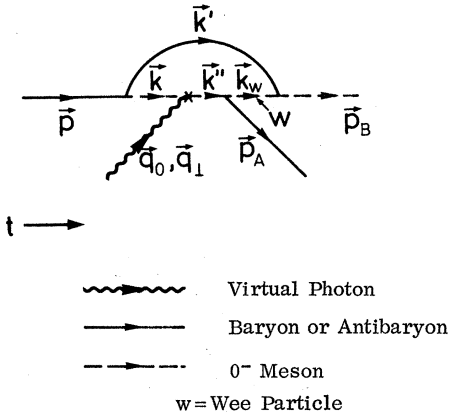

FIG. 17. Specific diagram for single-pion electroproduction (see Appendix C).

both the two other final nonwee particles are fermions. For either vertex we obtain the following factors: $q_\perp^{-1}$ from the wee-particle-containing energy denominator, $\sqrt{q_\perp}$ from the normalization of the wee particle, and $\sqrt{q_\perp}$ from only one of the fermions in a fermion-meson vertex being wee. Hence each vertex is $q_\perp$-independent. In case (b) $l_\alpha = 1$, $l_\beta = 3$, B is a meson, but the wee particle is a fermion; for the f vertex the other nonwee particle is a fermion but, for the h vertices drawn, the three other external nonwee particles consist of two mesons and one fermion. The f vertex is proportional to $\sqrt{q_\perp^{-1}}$ and among the h vertices the one to the left is proportional to $\sqrt{q_\perp^{-1}}$ whereas the other one (which has two wee-particle-containing energy denominators) goes as $\sqrt{q_\perp^{-3}}$ and is nonleading. Hence, once again, the leading $q_\perp$-dependence possible for $h_{p_B}^{l_\beta, l_\alpha}$ is the same as that of $f_{p_B}^{l_\alpha}$.

APPENDIX C: EXPLICIT VERIFICATION OF POWER-COUNTING TECHNIQUE FOR A SPECIFIC DIAGRAM

Consider the time-ordered diagram shown in Fig. 17 for single-pion electroproduction. Let g be the effective pion-nucleon coupling constant. We use E_k for the energy of a particle with momentum $\vec{k}$, and M and m stand for the nucleon and pion masses, respectively. Now

$$A \equiv (2\pi)^{9/2} \langle p_A, p_B \,\text{out} | J_{0,3} | p \rangle$$

$$= \frac{g^3 M}{\sqrt{2E_p F_{p_A} E_{p_B}}} \int \frac{d^3k'}{(2\pi)^3} \frac{1}{E - E_k - E_{k'}} \frac{1}{2E_{k'}} \frac{1}{2E_k} \frac{E_k + E_{k''}}{2E_{k''}} \frac{1}{q_0 + E_p - E_{k'} - E_{k''}} \frac{1}{2E_{k_w}} \frac{1}{E_p + q_0 - E_{p_A} - E_{k_w} - E_{k'}}$$

$$\times \sum_{s_w, s'} \bar{u}(\vec{p}_A)\gamma_5 v^{(s_w)}(\vec{k}_w)\bar{v}^{(s_w)}(\vec{k}_w)\gamma_5 u^{(s')}(\vec{k}')\bar{u}^{(s')}(\vec{k}')\gamma_5 u(\vec{p}) .$$

Here s_w, s' stand for internal spins which are being summed.

In the infinite-momentum frame introduced in Sec. II, we can write

$$\vec{p} = P\hat{z} ,$$

$$\vec{k} = \eta\vec{P} + \vec{k}_\perp \quad (0 < \eta < 1, \quad \vec{k}_\perp \cdot \hat{z} = 0),$$

$$\vec{k}' = (1 - \eta)\vec{P} - \vec{k}_\perp ,$$

$$\vec{k}'' = \eta\vec{P} + \vec{k}_\perp + \vec{q}_\perp ,$$

$$\vec{p}_A = \chi(\eta\vec{P} + \vec{k}_\perp + \vec{q}_\perp) - \vec{p}' \quad [0 < \chi < 1, \quad \vec{p}' \cdot (\eta\vec{P} + \vec{k}_\perp + \vec{q}_\perp) = 0] ,$$

$$\vec{k}_w = (1 - \chi)(\eta\vec{P} + \vec{k}_\perp + \vec{q}_\perp) + \vec{p}' ,$$

$$\vec{p}_B = (1 - \chi\eta)\vec{P} - \chi\vec{k}_\perp + (1 - \chi)\vec{q}_\perp + \vec{p}' .$$

Hence

$$E_p - E_k - E_{k'} = (2P)^{-1}[M^2 - (k_\perp^2 + m^2)\eta^{-1}(1 - \eta)^{-1}] ,$$

$$q_0 + E_p - E_{k'} - E_{k''} = (2P)^{-1}[2M\nu + M^2 - (k_\perp^2 + m^2)\eta^{-1}(1 - \eta)^{-1} - 2\vec{k}_\perp \cdot \vec{q}_\perp \eta^{-1} - q_\perp^2 \eta^{-1}] ,$$

and

$$q_0 + E_p - E_{p_A} - E_{k'} - E_{k_w} = (2P)^{-1}[2M\nu + M^2 - (\vec{k}_\perp + \vec{q}_\perp)^2\eta^{-1}(m^2 + p'^2 + \cdots)(1 - \chi)^{-1}\eta^{-1}$$
$$- (k_\perp^2 + m^2)(1 - \eta)^{-1} - (m^2 + p'^2 + \cdots)\chi^{-1}\eta^{-1}] .$$

We also have

$$X_A = \chi\eta \quad [\text{see Eq. (3.5a)}] ,$$

and

$$\lim_{q_\perp \to \infty} (1 - \chi) q_\perp = O(\mu) ,$$

$$\lim_{q_\perp \to \infty} X_A = \omega^{-1} \quad [\text{see Eq. (3.9)}] .$$

Hence, as in Sec. V, we can substitute $\eta = \omega^{-1}(1 + \mu q_\perp^{-1} z)^{-1}$ and replace $\int_0^1 d\eta$ by $\omega^{-1}\mu q_\perp^{-1} \int_0^{\text{finite}} dz$. Then we have

$$\lim_{\omega} A \simeq \frac{g^3}{\sqrt{8P}} \frac{1}{[\omega^{-1}(1-\omega^{-1})]^{1/2}} \left(\frac{1}{2\pi}\right)^3 \frac{\mu}{\omega q_\perp}$$
$$\times \int_0^{\text{finite}} dz \int d^2k_\perp \frac{1}{M^2 - \dfrac{k_\perp^2+m^2}{\omega^{-1}(1-\omega^{-1})}} \frac{1}{\omega^{-1}(1-\omega^{-1})} \frac{1}{M^2 - mq_\perp z\omega - \dfrac{k_\perp^2+m^2}{\omega^{-1}(1-\omega^{-1})}}$$
$$\times \frac{q_\perp}{mz\omega^{-1} + O(q_\perp^{-1})} \frac{1}{M^2 - mq_\perp z\omega - m\omega q_\perp z^{-1} - \dfrac{k_\perp^2}{1-\omega^{-1}} - M^2\omega - (p'^2 + \cdots)\dfrac{\omega q_\perp}{mz}} \text{(spinor part)}.$$

It is now easy to see that each energy denominator coming after the interaction of the virtual photon gives a factor of $q_\perp^{-1}$, the loop (containing a wee particle) generates another factor of $q_\perp^{-1}$, the "wee" internal line supplies a factor of $q_\perp$ and the spinor part [following Eq. (9) in the second paper of Ref. 3] contains a factor of $q_\perp$ coming from the wee internal nucleon. Thus $A \propto q_\perp^{-1}$ when $q_\perp \to \infty$, as given by the power-counting argument of footnote 19.

---

*Supported in part by the National Science Foundation.

†Address after Sept. 1, 1971: CERN, 1211 Geneva 23, Switzerland.

[1]R. P. Feynman, in *High Energy Collisions,* Third International Conference held at State University of New York, Stony Brook, 1969, edited by C. N. Yang, J. A. Cole, M. Good, R. Hwa, and J. Lee-Franzini (Gordon and Breach, New York, 1969); J. D. Bjorken and E. Paschos, Phys. Rev. 185, 1975 (1969).

[2]For informative reviews see E. Paschos, in *High Energy Physics,* edited by K. T. Mahanthappa, W. D. Walker, and W. E. Brittin (Colorado Associated Univ. Press, Boulder, 1970), and S. D. Drell, in *Proceedings of the International School of Physics "Ettore Majorana" Course 7,* edited by A. Zichichi (Academic Press, New York).

[3]S. D. Drell, D. J. Levy, and T.-M. Yan, Phys. Rev. 187, 2159 (1969); Phys. Rev. D 1, 1035 (1970); 1, 1617 (1970); S. D. Drell and T.-M. Yan, *ibid.* 1, 2402 (1970).

[4]See also S. D. Drell and T.-M. Yan, Phys. Rev. Letters 24, 855 (1970); 25, 316 (1970).

[5]For a lucid discussion of the contrasting dynamical roles of "wee" and "nonwee" partons, see S. D. Drell and T.-M. Yan, Ann. Phys. (N.Y.) (to be published).

[6]S. D. Drell and T.-M. Yan, Phys. Rev. Letters 24, 181 (1970). A definitive test of this connection is yet to be made. At present the experimental results are consistent with a fit of $(1/\omega)(1-1/\omega)^3$ for $F_2(\omega)$ near $\omega = 1$ [J. Friedman *et al.*, SLAC Report No. SLAC-PUB-907 (unpublished)].

[7]The results of the present paper were briefly reported earlier [P. Roy, Phys. Letters 36B, 579 (1971)].

[8]For theoretical treatments of single-particle electroproduction at high energies but with low to moderate values of Q^2, see F. A. Berends, Phys. Rev. D 1, 2590 (1971). See also R. Manweiler and W. Schmidt, *ibid.* 3, 2752 (1971) and an exhaustive list of references therein.

[9]D. R. Yennie, private communication.

[10]The *raison d'être* for this cutoff is the observation of bounded transverse momenta in hadronic reactions even up to very high energies [J. de Beer *et al.*, Can J. Phys. 46, 737 (1968)].

[11]This is because, in the model of Ref. 3, a single bare parton cannot make a transition to a physical particle (see the discussion towards the end of the first paper in Ref. 3). Hence we must have at least three final hadrons in order to avoid any interaction between the electromagnetically scattered parton and the unscattered bunch.

[12]This can be achieved by considering only the "good" ($\mu = 0, 3$) components of the electromagnetic current. See the second paper in Ref. 3.

[13]In the fixed-ω limit the result $-2q\cdot p_A Q^{-2} = 1 + O(1/\sqrt{Q^2})$ means that in the laboratory frame we have

$$-2Q^{-2}[\nu\kappa_A - (\nu^2+Q^2)^{1/2}(\kappa_A^2 - M_A^2)^{1/2}\cos\theta_A]$$
$$= 1 + O(1/\sqrt{Q^2}) \text{ as } Q^2 \to \infty.$$

Since now $\kappa_A/\nu = 1 + O(1/\sqrt{\nu})$, we can write, after expanding the square roots binomially, $(1 + M_p^{-1}\omega\kappa_A)(1-\cos\theta_A) = O(1/\sqrt{\nu})$ which immediately leads to Eq. (3.13). In the fixed-τ_A limit the result $-M_p^{-1}\nu^{-1} q\cdot p_A = \tau_A + O(1/\sqrt{\nu})$ implies that in the lab frame we have

$$-M_p^{-1}\nu^{-1}[\nu\kappa_A - (\nu^2+Q^2)^{1/2}(\kappa_A^2 - M_A^2)^{1/2}\cos\theta_A]$$
$$= \tau_A + O(1/\sqrt{\nu}).$$

Since $Q^2/2M_p\nu$ is now $1 + O(1/\sqrt{\nu})$, binomial expansions of the square roots give $(1-\cos\theta_A)(1+\nu/M_p) = O(1/\sqrt{\nu})$ from which one can obtain Eq. (3.19) directly.

[14]See the discussion in the last section of the first paper in Ref. 3 and also footnote 11 of the present paper.

[15]Cf. Eqs. (7) and (8) in the first paper of Ref. 4 and Eq. (7) in the second paper of the same. For the situation described in Fig. 5, the U-matrix formalism does not apply in a simple way. However, in this case, the existence of Eq. (5.8) with appropriately extended definitions of $g_{p_A}^{l\alpha}$ and $h_{p_B}^{l_\beta, l_\alpha}$ can be inferred from direct perturbative analyses of diagrams such as Fig. 14.

[16]Note that the lack of spin averaging is immaterial here since in the $P \to \infty$ frame the operators $j^{0,3}$ conserve helicity in the leading terms.

[17]For a spin-$\frac{1}{2}$ baryon F_1 is meant and for a neutral particle the electromagnetic form factor of its charged isospin partner.

[18]For some special vertices contributing to $h_{p_B}^{l_\beta, l_\alpha}$, the corresponding vertex for $f_{p_B}^{l\alpha}$ or $f_{p_B}^{l\beta}$ (as the case may be) may vanish because of symmetry requirements. For example, this happens in the model of Ref. 3 when B is a π meson and the "wee" partons are an odd number of pions (see also the discussion at the end of Sec. IV). Once again we assume that this small subset of "anom-

alous" diagrams makes no difference to our general argument.

[19]For any time-ordered single-particle electroproduction diagram, the leading power of $q_\perp^{-1}$ in the $q_\perp \to \infty$ limit can be checked following the general power-counting method described in Sec. IV in connection with elastic *ep* scattering. The only subtlety in the present case is the proper identification of each of the intermediate states that contributes a factor $\propto q_\perp^{-1}$ to the diagram from its energy denominator. Any intermediate state that appears after the interaction of the virtual photon and before the absorption of the last wee parton has to be included independent of whether it contains a wee particle or not. In the energy denominator of such a state the terms proportional to $q_\perp^2$ cancel out because of over-all energy conservation, but the terms proportional to $q_\perp$ persist. See the particular example in Appendix C.

[20]This buttresses our claim made towards the beginning of Sec. V that the external spin factors do not affect the leading $q_\perp$ dependence.

[21]These examples are not expected to give the correct $q_\perp$ dependences for the corresponding physical processes. Only their general feature is being used to propose a relation between W_2 and $[F]^2$.

[22]T. D. Lee, Ann. Phys. (N.Y.) (to be published).

[23]Y. Frishman, V. Rittenberg, H. R. Rubinstein, and S. Yankielowicz, Phys. Rev. Letters 26, 798 (1971). See also V. F. Müller and W. Ruhl, Nucl. Phys. B30, 513 (1971).

PHYSICAL REVIEW D VOLUME 5, NUMBER 1 1 JANUARY 1972

SU(3)×SU(3) Symmetry and K_{l3} Decays*

V. S. Mathur and T. C. Yang†
Department of Physics and Astronomy, University of Rochester, Rochester, New York 14627
(Received 13 September 1971)

The problem of the quadratic dependence on momentum transfer of the form factors in K_{l3} decay is analyzed. Assuming that the $(3, 3^*) + (3^*, 3)$ model provides a reasonable description of approximate SU(3)×SU(3) symmetry, several new sum rules have been written down which involve form factors defined at different momentum transfers. A solution of the various K_{l3} parameters is obtained and discussed.

I. INTRODUCTION

There has been a great deal of discussion recently[1] on the validity of the soft-pion theorem[2] in K_{l3} decays. The difficulty arises because the soft-pion theorem relates form factors evaluated at the momentum transfer $t = m_K^2$, which lies far beyond the physical region $m_l^2 \leq t \leq (m_K - m_\pi)^2$. Thus in order to test such a relation, one necessarily runs into the problem of momentum dependence of the form factors in the unphysical region. It has been customary to assume a linear t dependence of the form factors and indeed such a linear dependence seems to be consistent with the present experimental data.[1] However, if this linear relationship is extrapolated to the unphysical region, the experimental results seem to contradict the soft-pion theorem. A possible way out is that the form factors as a function of t may have nonlinear terms, which may be relatively unimportant in the physical region, but may become sizable in the extrapolated region near $t \sim m_K^2$. This paper deals with an investigation of this possibility.

Theoretically, one can study the momentum dependence of the form factors through the use of dispersion theory. In this case, inevitably, two problems arise. The first problem has to do with the number of subtractions to be used in the dispersion relations, or the knowledge of the asymptotic behavior of the form factors, about which very little is known. The second problem arises in evaluating the absorptive part of the form factors, for which one usually assumes pole dominance. Since the K^* and κ poles are rather far removed from the K_{l3} decay region of interest, it is not quite clear how good this assumption is.[3]

In this paper, we avoid dispersion theory and instead parametrize the t dependence of the form factors, retaining, however, the quadratic terms in t^2, which are generally ignored. The K_{l3} problem is then studied solely within the framework of chiral SU(3)×SU(3) symmetry. Such an investigation has many advantages, and in particular it serves to sharpen the experimental confrontation of our ideas regarding chiral SU(3)×SU(3) symmetry and its breaking. Our attitude in this paper will be to start with the idea that SU(3)×SU(3) symmetry realized through an octet of pseudoscalar Goldstone bosons, is indeed a reasonable approximate description of nature. Based on this description, two sum rules relevant to K_{l3} decays are well known: the usual soft-pion SU(2)×SU(2) theorem[2] and the Dashen-Weinstein relation.[4] A third soft-pion SU(3)×SU(3) sum rule has also been obtained by us[5] recently. To investigate the quadratic dependence on momentum transfer of the form factors, clearly more information is required. In this paper we derive what we believe is a maximal